

**Analysis of neuronal responses against  
disruption of paranodal junction**

**Kunisawa, Kazuo**

**DOCTOR OF PHILOSOPHY**

SOKENDAI (The Graduate University for Advanced Studies)

School of Life Science

Department of Physiological Sciences

**2016**

## **Acknowledgement**

Foremost, I would like to express my sincere gratitude to my advisor Prof. Kazuhiro Ikenaka of National Institute for Physiological Sciences for providing me an opportunity to conduct graduate study in his laboratory. I appreciate his continuous supports during my study and research, bonhomie, motivation, enthusiasm, and immense knowledge, which guided me throughout my research and writing this thesis.

I also would like to express my special appreciation to Dr. Takeshi Shimizu, Assistant Professor in National Institute for Physiological Sciences, who has been my supervisor since the beginning of my study. He provided me with a lot of helpful suggestion, important advice and guidance during the course of my work. He has devoted his precious time and made valuable suggestions that indeed helped to improve my thesis.

Special thanks are expressed to Prof. Norio Ozaki, Prof. Hiroko Baba, Prof. Manzoor A. Bhat, Dr. Itaru Kushima, Dr. Nobuhiko Hatanaka, Dr. Akiko Hayashi and Dr. Kenta Kobayashi for providing me numerous ideas, opportunity to do experiment in their laboratories, noble materials, relevant discussions, and teaching me their sophisticated techniques during my research work.

I would also like to thank the members of my thesis committee; Prof. Yumiko Yoshimura, Prof. Atsushi Nambu, and Prof. Kazunobu Sawamoto for their encouragement and insightful comments.

I appreciate all members in Prof. K. Ikenaka's laboratory: Dr. Takeshi Yoshimura,

Dr. Naoko Inamura, Dr. Shouta Sugio, Dr. Wilaiwan Wisessmith, Dr. Hirokazu Hashimoto, Jiang Wen, Mai Handa, Jiayi Li and Saori Kikuchihara for stimulating discussions and for a good time in Ikenaka's laboratory. I am deeply grateful to Dr. Yasuyuki Osanai and Rie Taguchi for giving me continuous supports and encouragement as members of the same research group in Ikenaka's laboratory.

I want to thank the people who support me during my doctoral course in Okazaki.

## **Table of contents**

Contents	4
Abbreviations	5
Abstract	6
Introduction	8
Materials and Methods	11
Results	21
Discussion	30
References	35
Figure legends	49
Table	56
Figures	57

## **Abbreviations**

AAV: Adeno-associated virus

Aqp3: Aquaporin 3

CST: Cerebroside sulfotransferase

CNS: Central nervous system

CNV: Copy number variant

Dcn: Decorin

Dct: Dopachrome tautomerase

EMG: Electromyogram

MRI: Magnetic resonance imaging

MS: Multiple sclerosis

Myh11: Myosin heavy polypeptide

NF155: Neurofascin155

PDGFR-  $\alpha$  : Platelet-derived growth factor receptor  $\alpha$

PLP: proteolipid protein

Pttg1: Pituitary tumor-transforming gene 1

ROS: Reactive oxygen species

Tti2: TELO2 interacting protein 2

vg: viral genome

## Abstract

Myelinated axons segregate the axonal membrane into four defined regions: the node of Ranvier, paranode, juxtaparanode and internode. The paranodal junction consists of their specific component proteins, such as neurofascin155 (NF155) on the glial side, and Caspr and contactin on the axonal side. Although myelin internodes are thought to have crucial roles in cognition and motor functions, the role of paranodal junction in neuronal responses remains unclear.

In the previous study, *Plp-CreERT* recombinase-induced ablation of *NF155* in oligodendrocytes (*Plp-CreERT;NF155<sup>Flox/Flox</sup>* mouse) led to disorganization of paranodal junctions. In this study, to determine whether site-directed loss of paranodal junctions affect the latency *in vivo*, I injected adeno-associated virus type5 (AAV5) harboring EGFP-2A-Cre into the internal capsule of *NF155<sup>Flox/Flox</sup>* mice, which led to disruption of paranodal junctions in a portion of pyramidal tract. I observed electromyogram and measured latency in response to electric stimulation of the motor cortex. Electrophysiological analysis showed that the latency was significantly delayed in *NF155<sup>Flox/Flox</sup>* mice injected with AAV5-EGFP-2A-Cre, compared to the control mice. These results demonstrate that the motor system outputs were affected by focal ablation of the paranodal junctions.

To further examine whether disruption of paranodal junctions affect neuronal gene expression, I prepared total RNA from the retina of *Plp-CreERT;NF155<sup>Flox/Flox</sup>* mice and control mice, and proceeded to microarray analysis. I found that expression

level of various neuronal genes dramatically changed in response to the ablation of paranodal junctions. Interestingly, the expression of some of the genes were significantly higher than that of control in *Plp-CreERT;NF155<sup>Flox/Flox</sup>* mice, but not in the cerebroside sulfotransferase knockout (*CST-KO*) mice, whose paranode has not been originally formed throughout their development. These results suggest that some neuronal genes are sensitive to an early change in the myelin-axon interaction during demyelination, such as paranodal opening.

Copy number variant (CNV) have been associated with susceptibility to schizophrenia. Since the disruption of paranodal junctions has been implicated in behavioral abnormalities related to schizophrenia, I examined whether there were consistency between the candidate genes identified with microarray analysis and CNV data of schizophrenia. I found that rare duplications of *aquaporin3*, whose expression was also influenced by paranodal opening, were observed in schizophrenia patients.

This study provides a new insight into the physiological function of paranodes.

## **Introduction**

Oligodendrocytes are glial cells that myelinate neuronal axons in the central nervous system (CNS). Myelin insulates axons to increase conduction velocity of neuronal action potentials (Waxman et al., 2005). Myelin is also important for neuronal maintenance because oligodendrocytes metabolically support axons through transport of lactate or pyruvate (Nave, 2010; Lee et al., 2012). Recently, Yamazaki et al. (2010) showed that depolarization of oligodendrocyte modulates conduction velocity of the axons it myelinates. Therefore, it is possible that oligodendrocytes/myelin actively communicate with axons, and thus might modulate various properties of neurons.

Myelinating process induces a dynamic change in axonal membrane protein localization, and segregates the axonal surface into four distinct segments: the node of Ranvier, the paranode, the juxtaparanode, and the internode (Peles et al., 2000). The paranodal region is unique in its ultrastructural characteristics and specific axo-glial junction (Einheber et al., 1997; Pedraza et al., 2001). These junctions are composed of three major paranodal proteins: 155-kD isoform of neurofascin (NF155; Volkmer et al., 1992; Charles et al., 2002) on the glial side, and Caspr (Einheber et al., 1997; Bhat et al., 2001) and a GPI-anchored neural cell adhesion molecule contactin (Berglund et al., 1999) on the axonal side. Paranodal junctions are thought to execute several functions: maintenance of conduction velocity propagation (Rasband et al., 1999), segregation of the axonal surface proteins (Rios et al., 2003), and signal transduction between axon and glia (Michailov et al., 2004).

Loss of central myelin is a major causative factor for neuronal dysfunctions and neurodegeneration in demyelinating diseases, including multiple sclerosis (MS; Dutta et al., 2011; Liu et al., 2012). MS patients frequently display cognitive impairments and psychiatric symptoms (Calabrese et al., 2009; Rahn et al., 2012). Paranodal opening occurs during the early phase of MS (Howell et al., 2006). Importantly, a previous study reported from our laboratory showed that the disruption of paranodal junctions led to abnormal behavior in the mouse related to schizophrenia (Tanaka et al., 2009). Magnetic resonance imaging (MRI) is a valuable tool to study region-specific alterations in psychiatric patient brain (Giedd et al., 2010). Previous MRI data showed that local and restricted structural changes within the white matter were observed in schizophrenia patient (Federspiel et al., 2006; Bai et al., 2009), suggesting that the focal abnormalities might also influence brain function. Pyramidal tract, a major motor pathway, has long-range connections through two synapses towards the peripheral nervous system (Jang, 2014). I hypothesized that the focal disruption of paranodal junctions eventually influences motor system outputs. Therefore, I investigated whether focal loss of paranodal junctions in the pyramidal tract affects the electrophysiological properties of motor system *in vivo*. I performed adeno-associated virus (AAV)-mediated site-specific ablation of the paranodal junctions in the tract. I observed electromyogram (EMG) and measured latency in response to electric stimulation of the motor cortex. Electrophysiological measurements revealed that focal disruption of paranodal junctions affected the latency of the entire system.

Interestingly, conduction velocity deficits influenced the expression of

oligodendroglial and neuronal genes (Roussos et al., 2012). This study may further suggest that the disruption of oligodendroglial paranodal junctions influences its counterpart axon, eventually affecting neuronal gene expression. To address this issue, I took advantage of conditional ablation of *NF155* in myelinating oligodendrocytes (*Plp-CreERT;NF155<sup>Flox/Flox</sup>* mouse, Doerflinger et al., 2003; Pillai et al., 2009). The mouse displays a gradual loss of paranodal junctions and a concomitant disorganization of axonal domains (Pillai et al., 2009). To determine whether the expression of neuronal genes is altered in response to the loss of paranodal junctions, I prepared total RNA from *Plp-CreERT;NF155<sup>Flox/Flox</sup>* mice and performed microarray analysis. I found that expression level of various neuronal genes changed in response to the ablation of paranodal junctions. Copy number variant (CNV), a major source of genetic variation in the human genome, contributes to the identification of the susceptibility genes for schizophrenia (Stewart et al. 2011). Next, I examined the relationship between the candidate genes identified with microarray analysis and CNV genes found in schizophrenia patients. Coincident genes between my microarray analysis and schizophrenic CNVs may play important roles in the pathogenesis of schizophrenia. Thus, this study provides a new insight into therapeutic approaches to neurological and psychiatric disorders by protecting neuronal dysfunction caused by paranodal abnormality.

## Materials and Methods

### Animals

C57BL/6J mice were obtained from Japan SLC Inc. (Hamamatsu, Japan). Transgenic mice used in this study were generated and genotyped as described previously: *Plp-CreERT;NF155<sup>Flox/Flox</sup>* (Doerflinger et al., 2003; Pillai et al., 2009); cerebroside sulfotransferase knockout (*CST-KO*, Ishibashi et al., 2002; Honke et al., 2002). *Plp-CreERT;NF155<sup>Flox/Flox</sup>* mice and the tissues obtained from *CST-KO* mice were kindly provided by Dr. Manzoor A. Bhat (University of Texas Health Science Center) and Dr. Hiroko Baba (Tokyo University of Pharmacy and Life Sciences), respectively. All procedures were conducted in accordance with the guidelines described by National Institutes of Health Guide for the Care and Use of Laboratory Animals, and the National Institute for Physiological Sciences Animal care and Use Committee.

### Tamoxifen treatment

Tamoxifen administration experiments were carried out according to the previous report (Doerflinger et al. 2003). In brief, Tamoxifen (Wako, Osaka, Japan) was dissolved at 10 mg/ml in sunflower oil by sonicating at 36°C for 30 minutes. *Plp-CreERT;NF155<sup>+ /Flox</sup>* or *Plp-CreERT;NF155<sup>Flox/Flox</sup>* mice were intraperitoneally

injected with 10 mg/ml tamoxifen for 10 consecutive days beginning at P23. I refer to them as *Plp-NF155<sup>Flox/Flox</sup>* and the *Plp-NF155<sup>+/Flox</sup>* mice, respectively. The animals were then sacrificed at various time points as described in the RESULTS section.

### **Mouse tissue preparation**

Mice were anesthetized and perfused transcardially with 4% paraformaldehyde in 0.1M phosphate buffer (pH. 7.4). Brains were post-fixed in 4% paraformaldehyde overnight at 4°C. The optic nerves were post-fixed in 4% paraformaldehyde for 1 min at room temperature. The post-fixed tissues were cryoprotected in PBS containing 20% sucrose overnight, embedded in OCT compound (Sakura Finetechnical Co., Tokyo, Japan), and cut into 20 µm (brains) or 10 µm (optic nerves) slices by cryostat (Leica CM3050, Wetzlar, Germany) for *in situ* hybridization and immunohistochemistry.

### ***In situ* hybridization**

Digoxigenin (DIG)-labeled single stranded riboprobes for *Pttg1* (GenBank Accession Number, BC023324), *Aqp3* (GenBank Accession Number, NM\_016689), *NM\_013917.2*, and *Plp1* (Kagawa et al., 1994) were synthesized using T7 RNA polymerase and DIG RNA labeling mix (Roche, Mannheim, Germany). The protocol for *in situ* hybridization was previously described (Ma et al., 2006). Briefly, the sections were treated with proteinase K (40 µg/ml for 30 min at room temperature) and

hybridized overnight at 60°C with DIG-labeled antisense riboprobes in a hybridization solution consisting of 40% formamide, 20mM Tris-HCl (pH 7.5), 600mM NaCl, 1mM EDTA, 10% dextran sulfate, 200 µg/ml yeast tRNA, 1x Denhardt's solution, and 0.25% SDS. The sections were washed three times in 1x SSC (150 mM NaCl and 15 mM trisodium citrate) containing 50% formamide at 60°C, followed by 0.1 M maleic buffer (pH 7.5) containing 0.1% Tween 20 and 0.15M NaCl. The bound DIG-labeled probe was detected by overnight incubation of the sections with anti-DIG antibody conjugated to alkaline phosphatase (Roche), and the color was developed in the solution containing 4-nitro-blue tetrazolium chloride (NBT, Roche) and 5-bromo-4-chloro-3-indolyl phosphate (BCIP, Roche) in the dark at room temperature.

### **Immunohistochemistry**

Cryosections were immunostained with mouse anti-pan Na<sup>+</sup> channel antibody (Sigma, St. Louis, USA), and rabbit anti-NF155 antibody (a gift from Dr. Hiroko Baba, Tokyo University of Pharmacy and Life Sciences, Japan) or rabbit anti-Caspr antibody (a gift from Dr. Elior Peles, Weizmann Institute of Science, Israel). Sections were irradiated in a microwave for 5 min in 10 mM citrate buffer, pH 6.0, heated to >90°C. After washing with PBS containing 0.1% Triton-X (PBST), sections were blocked with 10% normal goat serum in PBST for 1 h, then incubated with mouse anti-pan Na<sup>+</sup> channel antibody (1:500), and rabbit anti-NF155 antibody (1:500), or rabbit anti-Caspr antibody (1:1000) in PBST at 4°C overnight. After washing with PBST, the sections

were incubated with the secondary antibodies (1:2000, Alexa488-conjugated goat anti-rabbit IgG and Alexa568-conjugated goat anti-mouse IgG; Molecular Probes, Eugene, USA) and Hoechst 33342 (0.1 µg/ml; Sigma) for 3 h at room temperature. Sections were mounted and covered by glass coverslips after rinsing with PBST.

Sections used for *in situ* hybridization were also used for immunohistochemical analysis using 3,3'-diaminobenzidine (DAB) staining. The sections were blocked with 10% normal goat serum in PBST for 30 min and incubated with mouse anti-NeuN antibody (1:1000; Millipore, Billerica, USA) or rabbit anti-GFP antibody (1:500; Invitrogen, Eugene, USA) at 4°C overnight, followed by incubation with secondary antibodies (1:400, biotinylated goat anti-mouse IgG or biotinylated goat anti-rabbit IgG; Vector Laboratories, CA, USA) for 1 h at room temperature. After washing with PBST, sections were incubated with Avidin/Biotin Complex (ABC) solution (horseradish peroxidase-streptavidin-biotin complex, Vectastain ABC kit; Vector Laboratories) for 30 min at room temperature. The HRP signals were detected by DAB solution with 0.03% H<sub>2</sub>O<sub>2</sub>.

### **RT-PCR and qRT-PCR**

Total RNA was isolated using a Sepasol G kit (Nakarai, Kyoto, Japan) according to the manufacturer's instruction. The first-strand cDNA was synthesized using ReverTra Ace (Toyobo, Osaka, Japan). PCR was performed using KAPA Taq Extra PCR kit (Kapa Biosystems, Wilmington, USA). For the quantitative PCR, SYBR

Master Mix Reagent (Takara, Otsu, Japan) was used and then subjected to real time PCR quantification using the ABI7300 (Applied Biosystems, Waltham, USA). Quantitative PCR analysis was performed using a StepOne analyzer (Life Technologies, Carlsbad, USA). The PCR reaction program consists of 40 cycles of denaturation at 95 °C for 15 s, annealing at 60 °C for 30 s, and elongation at 72 °C for 1 min. To discriminate specific amplification from non-specific amplification, melting curve analysis was performed after each PCR reaction. To determine the starting cDNA amount, each purified PCR product with known concentrations was serially diluted and used as standards.  $\beta$ -actin was used as a housekeeping gene to normalize each PCR datum. All PCR primer sequences were described in Table 1.

### **Microarray analysis**

Total RNA prepared from mouse retina was isolated using NucleoSpin RNA kit (Takara) according to the manufacturer's instructions. The total RNA concentration was measured by NanoDrop spectrophotometrically. The quality of purified total RNA was verified by an Agilent 2100 bioanalyzer (Agilent technologies, Santa Clara, USA). Isolated total RNA was amplified and labeled as described in the One-Color Microarray-Based Gene Expression Microarrays Analysis Protocol (Agilent technologies). Briefly, total RNA (100 ng) was converted into cDNA using the Low Input Quick Amp Labeling Kit (Agilent technologies), followed by in vitro transcription and incorporation of Cyanine 3-CTP into cRNA. Cyanine 3-labeled cRNA was purified

using a RNeasy Mini kit (Qiagen, Hilden, Germany). After fragmentation, labelled cRNA was hybridized to SurePrint G3 Mouse Gene Expression 8x60K Microarray (Agilent Technologies) for 17 h at 65°C. The microarray was scanned by an Agilent Scanner, and the scan image data was analyzed with Feature Extraction software (Agilent Technologies). After background signal subtraction, the data for two microarray samples was managed and analyzed using the GeneSpring GX software (Agilent Technologies). There were a total of 55,821 probes used during the analysis for this technology. Raw intensity values were normalized to the 50 percentile shift and then submitted to a Bayesian correction based on the median of the control samples. Altered transcripts were identified using comparative method on the log<sub>2</sub> normalized intensity values between control and sample probes.

### **Preparation of AAV vectors**

EGFP-2A peptide-Cre cDNA was kindly provided by Dr. Akihiro Yamanaka (Nagoya University) and used as described previously (Inutsuka et al., 2014). All adeno-associated virus (AAV) vectors were produced and purified by Dr. Kenta Kobayashi according to the previously published methods (Matsushita et al., 1998, Okada et al., 2005). In brief, HEK293 cell ( $3 \times 10^6$  cells in 10 cm tissue culture dish) were cotransfected with pAAV vector plasmid harboring a gene of interest, pAAV-RC2, and pHelper (Cell Biolabs, Inc, San Diego, USA). The crude viral lysate was purified with 2 rounds of cesium chloride ultracentrifugation. The titer of the viral stock was

determined against plasmid standards by real-time PCR with primers 5'-CCGTTGTCAGGCAACGTG-3' and 5'-AGCTGACAGGTGGTGGCAAT-3'; subsequently, the stock was dissolved in HN buffer (50 mM HEPES [pH7.4] and 0.15 M NaCl) before infection.

### **AAV injection into the mouse brain**

Surgeries for AAV injections were conducted under ketamine/xylazine (100 and 5 mg/kg, respectively, i.p.) anesthesia using a stereotaxic instrument (Narishige, Tokyo, Japan). To check infection efficiency among AAVs, AAV1, 5, 6, or DJ-GFP were stereotaxically injected into a forebrain region in close proximity to the corpus callosum of adult (8-weeks-old) male C57BL6 mice. For electrophysiological experiments, AAV5-EGFP-2A-Cre was unilaterally injected into the internal capsule of 8-week-old *NF155<sup>Flox/Flox</sup>* mice. Injection sites were as follows: 1.0 mm posterior and 0.8 mm lateral to the bregma, at a depth of 1.0 mm, for AAV1, 5, 6, and DJ-GFP; 1.0 mm posterior and 2.1 mm lateral to the bregma, at a depth of 2.7 mm, for AAV5-EGFP-2A-Cre. After opening the skull around the injection site, 0.3 - 0.5  $\mu$ l of viral solution ( $1.0 - 3.0 \times 10^9$  viral genome (vg)) was injected through pulled glass pipettes (outer diameter 50 - 70  $\mu$ m) using air pressure.

### **Electrophysiology**

Seven-week-old *NF155<sup>Flox/Flox</sup>* mice were used for electrophysiological experiments. To painlessly fix the heads of awake mouse to a stereotaxic apparatus, mice received first surgical operation to install (or attach) prosthesis as described previously (Chiken et al., 2008). Briefly, each mouse was anesthetized with isoflurane (4%, 1 L/min with room air) and fixed in the stereotaxic apparatus. The skull was widely exposed and the periosteum and blood on the skull were completely removed. The exposed skull was completely covered with bone-adhesive resin (Bistite II; Tokuyama Dental, Tokyo, Japan) and acrylic resin (Unifast II; GC, Tokyo, Japan). A small polyacetal U-frame head holder for head fixation was mounted and fixed with acrylic resin on the head of the mouse. After recovery from the first surgery (2 or 3 d later), the mouse was positioned in the stereotaxic apparatus with its head restrained using the U-frame head holder under light anesthesia with isoflurane (2 %, 1 L/min with room air). A part of the skull in one hemisphere was removed to access the motor cortex. A bipolar stimulating electrode made of 50- $\mu$ m-diameter Teflon-coated tungsten wires (intertip distance, 300 - 400  $\mu$ m) was chronically implanted into the forearm representation area of the motor cortex, which was identified by intracortical microstimulation method (less than 50  $\mu$ A, 200  $\mu$ s duration at 333 Hz, 10 pulses). Then, a pair of electromyogram (EMG) recording electrode made of 50- $\mu$ m-diameter Teflon-coated stranded stainless steel wires was surgically placed in the triceps of forelimb under general anesthesia by isoflurane (2 %, 1 L/min with room air). The wires were passed subcutaneously and connected to connectors attached to the U-frame. After full recovery, the evoked EMG responses to the cortical stimulation were recorded

every week from seven to twenty week-old. The awake mouse was positioned in a stereotaxic apparatus using the U-frame head holder. Electrical stimulation was applied through the bipolar electrode implanted into motor cortex (0.6 mA, 100  $\mu$ s duration, single pulse, 1400 ms interval). The induced EMG signals were amplified (x5000), filtered (bandpass; 15-1000 Hz), rectified and stored on computer. The mean of EMG activity during the 0.5-s period preceding onset of the cortical stimulation was calculated, and the latency of responses was defined as the time which the cortically evoked activity exceeded the level of the mean + 2SD.

### **Extraction of genes affected by CNV**

In this study, I first obtained list of the copy number variant (CNV) identified in schizophrenia cases. CNV data was kindly provided by Prof. Norio Ozaki (Nagoya University) (Ikeda et al., 2010; Aleksic et al. 2013).

### **Data analyses**

All statistical analyses were performed and all figures produced with Prism 6 (GraphPad Software, Inc., San Diego, USA). Significant differences in comparisons of two groups were evaluated using Student's t-test. Multiple group comparisons were performed by one-way analysis of variance followed by Tukey's post hoc tests. The criterion for significant difference was  $p < 0.05$  in all statistical evaluations. All data are

presented as means  $\pm$  SEM.

## Results

### **Any serotype of AAV was applicable for labeling oligodendrocytes *in vivo***

Several studies indicated focal structural abnormalities in the white matter, linked to cognitive dysfunctions in schizophrenia patients (Lang et al., 2014). Therefore, it is possible that the focal disruption of paranodal junctions influence the outputs of its entire pathway. To address this issue, I employed an AAV-mediated focal ablation of *NF155* gene using the Cre-loxP system. Internal capsule is a part of the pyramidal tract and the most important motor pathway (Jang, 2014). Thus, I examined whether focal disruption of paranodal junction induced by site-directed *NF155* gene ablation in oligodendrocytes of internal capsule, affects motor system outputs *in vivo*. Stereotaxic injection of AAV harboring Cre recombinase (AAV-Cre) into the internal capsule was chosen to knock out the *NF155* gene because of its high titer and stability. AAV vectors have been widely used to transduce genes of interest into various kinds of tissues including CNS (McCown et al., 1996). However, there are no reports showing that AAV is capable for gene transfer into oligodendrocytes, in which *NF155* is expressed, in the adult mouse brain. Thus, I first determined which serotype of AAVs is able to infect oligodendrocytes in the forebrain. AAV-1, -5, -6, and -DJ harboring the GFP gene were injected into a forebrain region in close proximity to the corpus callosum (Fig. 1A). Three weeks after AAV injection, the mice were perfused. GFP expression

visualized showed that the stereotactic viral injections and subsequent gene transfer into the corpus callosum occurred properly (Fig. 1B). To determine whether oligodendrocytes were infected with AAV, sections applied with each serotype were double-labeled by *in situ* hybridization for oligodendrocyte marker *PLP* mRNA and immunostaining for GFP (Fig. 1C). The percentage of *PLP*<sup>+</sup> oligodendrocytes expressing GFP in the corpus callosum was shown in Figure 1D. AAV-DJ showed the highest average rate of  $51.6 \pm 12.5\%$ , followed by AAV-6 and AAV-5 at  $51.0 \pm 9.1\%$  and  $44.0 \pm 3.8\%$ , respectively. These results demonstrate that all AAV serotypes could label oligodendrocytes efficiently. Since AAV-5 requires platelet-derived growth factor receptor  $\alpha$  (PDGFR- $\alpha$ , which is specifically expressed in oligodendrocyte progenitor cells in the CNS (Pringle et al., 1992)) for its binding and gene transfer into the target cells (Kaludov et al., 2001), I used AAV-5 in the following experiments.

### **Reduction of latency in *NF155*<sup>Flox/Flox</sup> mice injected with AAV-Cre, analyzed by electrophysiology**

To examine whether the focal abnormality of paranodal junctions influences the electrophysiological property of motor system, I measured electromyogram (EMG) in response to electric stimulation of the motor cortex. I injected AAV5-EGFP-2A-Cre into the internal capsule of *NF155*<sup>Flox/Flox</sup> mice to focally eliminate paranodal junctions. Stimulating and recording electrodes were inserted into the motor cortex and forelimb

of 7-week-old  $NF155^{Flx/Flx}$  mice, respectively (Fig. 2A). One week later, AAV5-EGFP-2A-Cre was injected into the internal capsule of the mice (Fig. 2B). Wild-type mice were also treated in the same way, as a control. A typical response pattern of EMG evoked by the stimulation of motor cortex was shown in Figure 2C. I first confirmed whether AAV5-EGFP-2A-Cre injection into the internal capsule actually disrupted paranodal junctions (Fig. 3A). The sections were histologically examined 12 weeks after the AAV5-EGFP-2A-Cre injection. Double-labeling with *in situ* hybridization for *PLP* mRNA and immunostaining for GFP showed  $89.3 \pm 4.5\%$  co-localization of GFP expression with *PLP*<sup>+</sup> oligodendrocytes (Fig. 3B). To confirm loss of the paranodal junctions in the internal capsule, I also performed double immunofluorescence for Na<sup>+</sup> channels and Caspr. In the control mice, Na<sup>+</sup> channels were concentrated at the nodes of Ranvier, and Caspr were localized in the paranodal region (Fig. 3C). On the other hand, although Na<sup>+</sup> channel clusters were preserved at the nodes of Ranvier in the  $NF155^{Flx/Flx}$  mice, the length of Caspr clusters was significantly shorter than that in the control mice (Fig. 3C, D). This result demonstrated that the AAV5-EGFP-2A-Cre injection into the  $NF155^{Flx/Flx}$  mice efficiently induced an ablation of the paranodal junctions. To investigate whether focal disruption of paranodal junctions in the pyramidal tract affect latency in response to electric stimulation of the motor cortex, EMG was measured every week until 20-week-old. Figure 4 summarized latencies of both  $NF155^{Flx/Flx}$  and the control mice. As the control mice aged, the latency became progressively shorter. In contrast, latency in the  $NF155^{Flx/Flx}$  mice injected with AAV5-EGFP-2A-Cre was significantly prolonged,

compared to the control mice. These data indicate that the motor system outputs were influenced by the focal loss of paranodal junctions.

### **Disorganization of paranodal junctions in the optic nerve of *NF155* mutant mice**

Since the ablation of paranodal junctions influenced electrophysiological properties of the axon, it is possible that disruption of paranodal junctions affects gene expression in neuronal cells. To address this issue, I took advantage of a tamoxifen inducible-Cre line; Cre is specifically expressed in proteolipid protein (PLP)-positive mature oligodendrocytes (*Plp-CreERT*), leading to ablation of *NF155* gene during postnatal development in mature oligodendrocytes (*Plp-CreERT;NF155<sup>Flox/Flox</sup>* mouse, Doerflinger et al., 2003; Pillai et al., 2009). *Plp-CreERT;NF155<sup>Flox/Flox</sup>* and age-matched *Plp-CreERT;NF155<sup>+ /Flox</sup>* mice were intraperitoneally injected with tamoxifen for the 10 consecutive days, from P23 to P33. I refer to them as *Plp-NF155<sup>Flox/Flox</sup>* and the *Plp-NF155<sup>+ /Flox</sup>* mice, respectively (see Materials and Methods). To investigate neuronal gene expression in response to the loss of paranodal junctions, I applied Agilent GeneChip analysis for retinal tissue. The mouse retina contains neuronal cell bodies of optic nerve axons. In addition, myelin is absent in the retina because the astrocytes form a honeycomb-like structure that has been called lamina cribrosa adjacent to the retinal area. Therefore, it was useful to identify only the neuronal genes affected by the disruption of paranodal junctions. To confirm the loss of paranodal junctions in the optic nerves of *Plp-NF155<sup>Flox/Flox</sup>* mice, immunostaining for NF155 and

Caspr was performed in the optic nerves (Fig. 5A). In the *Plp-NF155<sup>Flox/Flox</sup>* mice 60 days after tamoxifen administration, the number and length of NF155 clusters were significantly reduced compared with the *Plp-NF155<sup>+/Flox</sup>* mice (Fig. 5B). I also observed apparent decrease of Caspr-positive paranodes in the optic nerves of *Plp-NF155<sup>Flox/Flox</sup>* mice 60 days after tamoxifen administration (Fig. 5C). These results are consistent with the previous studies showing that *NF155* mutants induce disruption of paranodal junctions in the peripheral nervous system (Pillai et al., 2009).

### **Expression profiles of neuronal genes in response to *NF155* ablation**

To examine gene expression profiles in the retina of *Plp-NF155<sup>Flox/Flox</sup>* mice, microarray analysis was performed with total retinal RNA isolated from *Plp-NF155<sup>+/Flox</sup>* or *Plp-NF155<sup>Flox/Flox</sup>* mice (n = 2 per group) 60 days after tamoxifen administration. Interestingly, microarray analysis revealed that expression level of various neuronal genes dramatically changed in response to the ablation of paranodal junctions (Fig. 6A). Expression levels of 433 genes showed more than two fold difference between the *Plp-NF155<sup>Flox/Flox</sup>* group and the *Plp-NF155<sup>+/Flox</sup>* group. Among the 433 genes, 228 genes were up-regulated and the remainders were down-regulated.

To validate the results obtained by microarray analysis, total RNA was extracted from the retina of *Plp-NF155<sup>Flox/Flox</sup>* mice and used for quantitative RT-PCR (qRT-PCR). Among the identified genes, I focused on six genes that could influence neuronal function and survival. These focused genes were indicated in Fig. 6A; decorin

(*Dcn*); myosin heavy polypeptide 11 (*Myh11*); pituitary tumor-transforming gene 1 (*Pttg1*); dopachrome tautomerase (*Dct*); TELO2 interacting protein 2 (*Tti2*) and aquaporin 3 (*Aqp3*). Among aforementioned genes, *Dcn* and *Myh11* are survival factors for neurons through TGF- $\beta$  and IGF-1 signaling (Iozzo et al., 2011; Renard et al., 2013), respectively. *Pttg1* and *Dct* are involved in tumor development (Lee et al., 1999; Pak et al., 2004), whereas *Tti2* is a regulator of DNA damage response (Hurov et al., 2010), and *Aqp3* functions to homeostatically maintain water molecule within the cell (Preston et al., 1992). The primers used for PCR amplification were listed in Table 1. Either up-regulation or down-regulation of these gene expression levels detected by qRT-PCR was comparable to those obtained with the microarray analysis, indicating that the microarray expression data were reliable (Fig. 6B, C). Together, these findings suggest that neuronal function is affected by altered gene expression caused by the collapse of paranodal junctions.

#### **Comparison of the identified gene expression in the retina between *Plp-NF155<sup>Flox/Flox</sup>* and *CST-KO* mice**

The microarray analysis indicated that the gradual loss of paranodal junctions induced altered gene expression. I next examined whether expression levels of the selected genes were also changed in another mutant mouse line whose paranodes have never been formed. A cerebroside sulfotransferase (CST) enzyme synthesizes sulfatide, a major lipid component of the myelin sheath (Eckhardt et al., 2007). Ishibashi et al.

(2002) reported that *CST* mutant mice do not form paranodal junctions throughout their development. The expression levels of the selected genes in the retina of 4- or 6-week-old *CST-KO* mice were compared to those of *Plp-NF155<sup>Flox/Flox</sup>* mice 40 or 60 days after tamoxifen administration. Similar to the results obtained in the *Plp-NF155<sup>Flox/Flox</sup>* mice, *Dcn* and *Myh11* expressions were also induced in the *CST-KO* mice (Fig. 7A-D). Interestingly, some genes responded in a distinct manner between *Plp-NF155<sup>Flox/Flox</sup>* and *CST-KO* mice. *Pttg1* and *Aqp3* expression was significantly altered only in the *Plp-NF155<sup>Flox/Flox</sup>* mice (Fig. 7E, G) but not in the *CST-KO* mice (Fig. 7F, H). Therefore, both consistent and inconsistent expression patterns of the selected genes were observed between these two different mouse models. These data also suggest that some genes immediately respond to the paranodal disruption only after the junction is formed.

***Pttg1* expression was changed in the *Plp-NF155<sup>Flox/Flox</sup>* cerebral cortex, but not in the *CST-KO***

Among the several genes validated by qRT-PCR, *Pttg1* was one of the highly up-regulated genes in the *Plp-NF155<sup>Flox/Flox</sup>* mouse retina. Therefore, I examined whether *Pttg1* expression was also induced in the cerebral cortex of *Plp-NF155<sup>Flox/Flox</sup>* or *CST-KO* mice. qRT-PCR analysis revealed over 4-fold up-regulation of *Pttg1* expression in the cortex of *Plp-NF155<sup>Flox/Flox</sup>* mice (Fig. 8A). On the other hand, the *Pttg1* mRNA levels did not increase in the *CST-KO* mice (Fig. 8B). Next, to examine

the cell types that express *Pttg1* in cerebral cortex, I performed immunostaining with cell lineage specific markers following *Pttg1 in situ* hybridization (Fig. 8C). About 70% of *Pttg1*<sup>+</sup> cells were positive for neuron marker NeuN, indicating that it was primarily expressed in neurons (Fig. 8D). These results demonstrate that neuronal gene expression is affected by the disruption of paranodal junctions in the cerebral cortex as well.

### **CNV screening exhibited deletion/duplication genes associated with schizophrenia**

Our previous findings demonstrated the schizophrenia-related behaviors accompanied by abnormal paranodal regions (Tanaka et al., 2009). CNV, a major source of genetic variation in the human genome, of some genes are linked to the risk for schizophrenia (Stewart et al. 2011). To further determine whether the genes identified by microarray analysis were linked to schizophrenia, I examined whether some of the genes identified in this study are present in the list of genes with CNV in the schizophrenic patients. Intriguingly, I found that some of the identified genes were also found in the rare CNV associated with schizophrenia. Among those genes, the locus encoding *Aqp3* displayed a characteristic CNV pattern. I found that chromosomal duplications of the *Aqp3* locus were frequently detected in schizophrenia patients (n=1699; Fig. 9A). To analyze *Aqp3* expression in the CNS, I examined the mRNA levels in the cerebral cortex. In the *Plp-NF155<sup>Flox/Flox</sup>* mice, qRT-PCR analysis showed significantly reduced expression of *Aqp3* (Fig. 9B). Furthermore, I found that some *Aqp3*<sup>+</sup> cells in the cerebral cortex were also positive for neuron marker NeuN (Fig. 9C).

About 53% of the *Aqp3*<sup>+</sup> cells were NeuN<sup>+</sup> neurons, detected by NeuN immunolabeling following *Aqp3 in situ* hybridization (Fig. 9D). Although it remains unclear whether the loss of paranodal junctions contribute to the risk of schizophrenia, these results suggest that insufficient reduction of *Aqp3* gene expression accompanying the disorganization may play important roles in pathogenesis of schizophrenia.

## **Discussion**

In this study, I found that focal disruption of paranodal junctions in the internal capsule caused a delay in the forelimb muscle response against stimulus of the motor cortex (Fig. 4), which contains two synaptic connections. My results further suggest that focal loss of paranodal junctions in other white matter area affects the electrophysiological properties of other systems as well. Action potential from different neural circuits is required to reach a target neuron simultaneously (Takahashi et al., 2011). If the conduction velocities of various axons are reduced to a different extent, synchronized input might be hardly achieved (Federspiel et al., 2006). Interestingly, genetic studies have demonstrated that abnormal expression of neuronal genes was associated with the disruption of the node of Ranvier (Katsel et al., 2004; Roussos et al., 2012). Therefore, the delayed latency caused by the focal disruption of paranodal junctions may affect neuronal gene expression.

Thus, I applied microarray analysis and qRT-PCR to explore neuronal genes that respond to the collapse of paranodal junctions in the mouse retina. The results revealed that over 400 genes were differentially up-regulated or down-regulated more than two fold from the control level (Fig. 6A). The retinal tissue was useful to identify neuronal genes affected by the disruption of paranodal junctions because myelin is absent in this tissue. MS is a demyelinating diseases characterized by both myelin loss and neuronal degeneration (Coman et al., 2006). Although the paranodal junctions are thought to be the initial damaged site in MS patients, influence of paranodal junction disruption on

neurons has yet to be elucidated (Howell et al., 2006). Importantly, paranodal junctions act as a seal between the myelin sheath and axon to separate from the extracellular environments (Bhat et al., 2001). Previous studies suggested that the structural abnormality of paranodes might allow reactive oxygen species (ROS) and proteases to invade into the internodal space (Gonsette, 2008; Rosenbluth et al., 2013). Oxidative stress is commonly implicated in the development of neurological pathology, and ROS contribute to several aspects of MS pathogenesis (Tezel, 2006; Ortiz et al., 2013). The accumulation of oxidative stress in the acute inflammatory lesions of MS leads to mitochondrial dysfunction (Trapp et al., 1998; Su et al., 2009; Takihara et al., 2015), which induces axonal injury and disrupted axonal transport (Rintoul et al., 2006; Su et al., 2009). Disruption of paranodal junctions in *Plp-NF155<sup>Flox/Flox</sup>* mice revealed cytoskeletal swellings along the axons (Pillai et al., 2009). In addition, organelle accumulation was found in the paranodal region flanked by the swelling lesions, a sign of disrupted axonal transport that eventually leads to axonal degeneration (Garcia-Fresco et al., 2006). Although the exact molecular mechanisms remain to be elucidated, these reports suggest that the disruption of paranodal junctions cause axonal transport deficits and induce cytotoxic stresses.

Consistent with these previous reports, there were differences in the expression profiles of many genes between *Plp-NF155<sup>Flox/Flox</sup>* and *CST-KO* mice. For example, the expression levels of *Pttg1* and *Aqp3* were altered in the *Plp-NF155<sup>Flox/Flox</sup>*, but remained unchanged in the *CST-KO* mice (Fig. 7E-H). These results suggest that some genes are sensitive to the paranodal disruption only after the junction was formed. It is unclear

how the gradual loss of paranodal junctions after its formation can be different from their loss throughout the development that results in the altered the gene expression responses. Microarray analysis of *CST-KO* mice in comparison with *Plp-NF155<sup>Flox/Flox</sup>* data might be helpful for us to identify molecular mechanisms underlying these different gene expressions.

I speculated that the expression of these identified genes do not change only in the retina but also in the brain in response to the ablation of paranodal junctions. I found that the expression of *Pttg1* in the cerebral cortex was significantly increased in *Plp-NF155<sup>Flox/Flox</sup>* mice compared with the *Plp-NF155<sup>+ / Flox</sup>* mice (Fig. 8A). Furthermore, *in situ* hybridization analysis revealed that *Pttg1*-positive signal was mostly colocalized with NeuN-positive neurons (Fig. 8C, D). These results suggest that the expression profiles obtained from retinal sample could be applied to other regions in the CNS. What is the functional role of *Pttg1* in the brain? The function of *Pttg1* in the CNS is still unknown. *Pttg1* is transcriptionally regulated by various growth factors and highly expressed in various kinds of tumors and tumor cell lines, thus defined as an oncogene (Panguluri et al., 2008). *Pttg1* is thought to play a role in cell proliferation (Zou et al., 1999), DNA damage/ repair (Romero et al., 2001), and cell transformation processes (Wang et al., 2003). Although the pathophysiological significance of *Pttg1* expression increase is unclear at present, *Pttg1* can serve as a good neuronal marker for the onset of paranodal opening. Further studies of the *Pttg1* functions in the *Plp-NF155<sup>Flox/Flox</sup>* mice will provide important insights on the roles of the gene regulation during the disruption of paranodal junctions.

Importantly, overexpression of proteolipid protein 1 (PLP), a major component of myelin sheath, causes an overall abnormality of CNS oligodendrocytes, including abnormal paranodal junctions (Tanaka et al., 2009). Our previous studies have reported that the PLP overexpressing mouse displayed various behavioral abnormalities in relation to cognitive dysfunction, which is one of the characteristic features of schizophrenia-like behaviors (Tanaka et al., 2009). Growing number of recent reports demonstrated the involvement of CNV in schizophrenia (McClellan et al., 2007). As one of the major sources of genetic variation, CNV provide versatile tools to identify promising candidate genes for schizophrenia (Luo et al., 2014). In this study, by comparing the microarray data to the list of genes with CNV, I was able to propose some of the susceptibility gene associated with schizophrenia have connections with the paranodal opening. Eight of the 1699 schizophrenia patients display rare duplications in the 9p13.3 region encompassing the *Aqp3* gene (Fig. 9A). Furthermore, my microarray data demonstrated that the disruption of paranodal junctions decreased *Aqp3* expression (Fig. 9B). *In situ* hybridization analysis further revealed that *Aqp3* gene was mainly expressed in neurons (Fig. 9C, D), consistent with the previous study (Yamamoto et al., 2001). *Aqp3* is a water-selective channel that increases plasma membrane water permeability of the cells (Preston et al., 1992). Interestingly, *Aqp3* facilitated cell proliferation by the mechanism involving ATP production (Verkman et al., 2008; Galán-Cobo et al., 2015). In addition, proliferation abnormalities of hippocampal neurons were observed in schizophrenia patients (Allen et al., 2015). These studies may suggest that functional abnormalities of the *Aqp3* gene are involved in schizophrenia

pathophysiology. I have no direct evidence showing that the paranodal junction defects were implicated in the onset of schizophrenia in this study. However, the identification of the promising candidate gene might open a new path towards future studies on schizophrenia-related genes. Further approaches for *Aqp3* gene function may provide new insights into the etiology of schizophrenia and potential therapeutic targets.

In conclusion, my present results revealed that focal ablation of paranodal junctions could result in a delay in the forelimb muscle response against stimulus of the motor cortex, indicating that focal abnormality in myelin-axon interaction can affect the electrophysiological property of entire system. In addition, I found that the gradual loss of paranodal junctions in *Plp-NF155<sup>Flox/Flox</sup>* mice induced altered neuronal gene expression. Interestingly, expression of some of the identified genes was unchanged in *CST-KO* mice, whose paranodes have never been formed throughout their development. These results suggest that the candidate genes identified in this study might help us to investigate neuronal functions affected by the disruption of paranodal junctions. According to the relation between the candidate genes identified with microarray analysis and CNV data of schizophrenia, *Aqp3* is a highly potential candidate gene that showed rare duplications in schizophrenia patients. These data may provide a new insight into the paranodal physiological function as a therapeutic target for psychiatric disorders.

## References

Aleksic B, Kushima I, Ohye T, Ikeda M, Kunimoto S, Nakamura Y, Yoshimi A, Koide T, Iritani S, Kurahashi H, Iwata N, Ozaki N. (2013). Definition and refinement of the 7q36.3 duplication region associated with schizophrenia. *Sci Rep* 3:2587.

Allen KM, Fung SJ, Shannon Weickert C. (2015). Cell proliferation is reduced in the hippocampus in schizophrenia. *Aust N Z J Psychiatry* pii:0004867415589793.

Bai YM, Chou KH, Lin CP, Chen IY, Li CT, Yang KC, Chou YH, Su TP. (2009). White matter abnormalities in schizophrenia patients with tardive dyskinesia: a diffusion tensor image study. *Schizophr Res* 109:167-181.

Berglund EO, Murai KK, Fredette B, Sekerkova G, Marturano B, Weber L, Mugnaini E, Ranscht B. (1999). Ataxia and abnormal cerebellar microorganization in mice with ablated contactin gene expression. *Neuron* 24:739-750.

Bhat MA, Rios JC, Lu Y, Garcia-Fresco GP, Ching W, St Martin M, Li J, Einheber S, Chesler M, Rosenbluth J, Salzer JL, Bellen HJ. (2001). Axon-glia interactions and the domain organization of myelinated axons requires neurexin IV/Caspr/Paranodin. *Neuron* 30:369-383.

Calabrese M, Agosta F, Rinaldi F, Mattisi I, Grossi P, Favaretto A, Atzori M, Bernardi V, Barachino L, Rinaldi L, Perini P, Gallo P, Filippi M. (2009). Cortical lesions and atrophy associated with cognitive impairment in relapsing-remitting multiple sclerosis. *Arch Neurol* 66:1144-1150.

Charles P, Tait S, Faivre-Sarrailh C, Barbin G, Gunn-Moore F, Denis-Nehrbass N, Guennoc AM, Girault JA, Brophy PJ, Lubetzki C. (2002). Neurofascin is a glial receptor for the paranodin/Caspr-contactin axonal complex at the axoglia junction. *Curr Biol* 12:217-220.

Chiken S, Shashidharan P, Nambu A. (2008). Cortically evoked long-lasting inhibition of pallidal neurons in a transgenic mouse model of dystonia. *J Neurosci* 28:13967-13977.

Coman I, Aigrot MS, Seilhean D, Reynolds R, Girault JA, Zalc B, Lubetzki C. (2006). Nodal, paranodal and juxtapanodal axonal proteins during demyelination and remyelination in multiple sclerosis. *Brain* 129:3186-3195.

Doerflinger NH, Macklin WB, Popko B. (2003). Inducible site-specific recombination in myelinating cells. *Genesis* 35:63-72.

Dutta R, Trapp BD. (2011). Mechanisms of neuronal dysfunction and degeneration in multiple sclerosis. *Prog Neurobiol* 93:1-12.

Eckhardt M, Hedayati KK, Pitsch J, Lüllmann-Rauch R, Beck H, Fewou SN, Gieselmann V. (2007). Sulfatide storage in neurons causes hyperexcitability and axonal degeneration in a mouse model of metachromatic leukodystrophy. *J Neurosci* 27:9009-9021.

Einheber S, Zanazzi G, Ching W, Scherer S, Milner TA, Peles E, Salzer JL. (1997). The axonal membrane protein Caspr, a homologue of neurexin IV, is a component of the septate-like paranodal junctions that assemble during myelination. *J Cell Biol* 139:1495-1506.

Federspiel A, Begre S, Kiefer C, Schroth G, Strik WK, Dierks T. (2006). Alterations of white matter connectivity in first episode schizophrenia. *Neurobiol Dis* 22:702-709.

Galán-Cobo A, Ramírez-Lorca R, Serna A, Echevarría M. (2015). Overexpression of AQP3 modifies the cell cycle and the proliferation rate of mammalian cells in culture. *PLoS One* 10:e0137692.

Garcia-Fresco GP, Sousa AD, Pillai AM, Moy SS, Crawley JN, Tessarollo L, Dupree

JL, Bhat MA. (2006). Disruption of axo-glial junctions causes cytoskeletal disorganization and degeneration of Purkinje neuron axons. *Proc Natl Acad Sci USA* 103:5137-5142.

Giedd JN, Rapoport JL. (2010). Structural MRI of pediatric brain development: what have we learned and where are we going? *Neuron* 67:728-734.

Gonsette RE. (2008). Oxidative stress and excitotoxicity: a therapeutic issue in multiple sclerosis? *Mult Scler* 14:22-34.

Honke K, Hirahara Y, Dupree J, Suzuki K, Popko B, Fukushima J, Nagasawa T, Yoshida N, Wada Y, Taniguchi N. (2002). Paranodal junction formation and spermatogenesis require sulfoglycolipids. *Proc Natl Acad Sci USA* 99:4227–4232.

Howell OW, Palser A, Polito A, Melrose S, Zonta B, Scheiermann C, Vora AJ, Brophy PJ, Reynolds R. (2006). Disruption of neurofascin localization reveals early changes preceding demyelination and remyelination in multiple sclerosis. *Brain* 129:3173-3185.

Hurov KE, Cotta-Ramusino C, Elledge SJ. (2010). A genetic screen identifies the Triple T complex required for DNA damage signaling and ATM and ATR stability. *Genes Dev* 24:1939-1950.

Ikeda M, Aleksic B, Kirov G, Kinoshita Y, Yamanouchi Y, Kitajima T, Kawashima K, Okochi T, Kishi T, Zaharieva I, Owen MJ, O'Donovan MC, Ozaki N, Iwata N. (2010). Copy number variation in schizophrenia in the Japanese population. *Biol Psychiatry* 67(3):283-286.

Inutsuka A, Inui A, Tabuchi S, Tsunematsu T, Lazarus M, Yamanaka A. (2014). Concurrent and robust regulation of feeding behaviors and metabolism by orexin neurons. *Neuropharmacology* 85:451-460.

Iozzo RV, Buraschi S, Genua M, Xu SQ, Solomides CC, Peiper SC, Gomella LG, Owens RC, Morrione A. (2011). Decorin antagonizes IGF receptor I (IGF-IR) function by interfering with IGF-IR activity and attenuating downstream signaling. *J Biol Chem* 286:34712-34721.

Ishibashi T, Dupree JL, Ikenaka K, Hirahara Y, Honke K, Peles E, Popko B, Suzuki K, Nishino H, Baba H. (2002). A myelin galactolipid, sulfatide, is essential for maintenance of ion channels on myelinated axon but not essential for initial cluster formation. *J Neurosci* 22:6507-6514.

Jang SH. (2014). The corticospinal tract from the viewpoint of brain rehabilitation. *J Rehabil Med* 46:193-199.

Kagawa T, Ikenaka K, Inoue Y, Kuriyama S, Tsujii T, Nakao J, Nakajima K, Aruga J, Okano H, Mikoshiba K. (1994). Glial cell degeneration and hypomyelination caused by overexpression of myelin proteolipid protein gene. *Neuron* 13:427-442.

Kaludov N, Brown KE, Walters RW, Zabner J, Chiorini JA. (2001). Adeno-associated virus serotype 4 (AAV4) and AAV5 both require sialic acid binding for hemagglutination and efficient transduction but differ in sialic acid linkage specificity. *J Virol* 75:6884-6893.

Katsel P, Dracheva S, Copland CM, Gorman JM, Davis KL, Haroutunian V. (2004). Tight and adherens junctions genes of myelinating oligodendrocytes are downregulated in schizophrenia. *Biol Psychiatry* 55(8)(suppl):159.

Lang DJ, Yip E, MacKay AL, Thornton AE, Vila-Rodriguez F, MacEwan GW, Kopala LC, Smith GN, Laule C, MacRae CB, Honer WG. (2014). 48 echo T<sub>2</sub> myelin imaging of white matter in first-episode schizophrenia: evidence for aberrant myelination. *Neuroimage Clin* 6:408-414.

Lee IA, Seong C, Choe IS. (1999). Cloning and expression of human cDNA encoding human homologue of pituitary tumor transforming gene. *Biochem Mol Biol Int* 47:891-897.

Lee Y, Morrison BM, Li Y, Lengacher S, Farah MH, Hoffman PN, Liu Y, Tsingalia A, Jin L, Zhang Ping-Wu, Pellerin L, Magistretti PJ, Rothstein JD. (2012). Oligodendroglia metabolically support axons and contribute to neurodegeneration. *Nature* 487:443-448.

Liu J, Dietz K, DeLoyht JM, Pedre X, Kelkar D, Kaur J, Vialou V, Lobo MK, Dietz DM, Nestler EJ, Dupree J, Casaccia P. (2012). Impaired adult myelination in the prefrontal cortex of socially isolated mice. *Nat Neurosci* 15:1621-1623.

Luo X, Huang L, Han L, Luo Z, Hu F, Tieu R, Gan L. (2014). Systematic prioritization and integrative analysis of copy number variations in schizophrenia reveal key schizophrenia susceptibility genes. *Schizophr Bull* 40:1285-1299.

Ma J, Matsumoto M, Tanaka KF, Takebayashi H, Ikenaka K. (2006). An animal model for late onset chronic demyelination disease caused by failed terminal differentiation of oligodendrocytes. *Neuron Glia Biology* 2:81-91.

Matsushita T, Elliger S, Elliger C, Podsakoff G, Villarreal L, Kurtzman GJ, Iwaki Y, Colosi P. (1998). Adeno-associate virus vectors can be efficiently produced without helper virus. *Gene therapy* 5:938-945.

McClellan JM, Susser E, King MC. (2007). Schizophrenia: a common disease caused

by multiple rare alleles. *Br J Psychiatry* 190:194-199.

McCown TJ, Xiao X, Li J, Breese GR, Samulski RJ. (1996). Differential and persistent expression patterns of CNS gene transfer by an adeno-associated virus (AAV) vector. *Brain Res* 713:99-107.

Michailov GV, Sereda MW, Brinkmann BG, Fischer TM, Haug B, Birchmeier C, Role L, Lai C, Schwab MH, Nave KA. (2004). Axonal neuregulin-1 regulates myelin sheath thickness. *Science* 304:700-703.

Nave KA. (2010). Myelination and support of axonal integrity by glia. *Nature* 468:244-252.

Okada T, Nomoto T, Yoshioka T, Nonaka-Sarukawa M, Ito T, Ogura T, Iwata-Okada M, Uchibori R, Shimazaki K, Mizukami H, Kume A, Ozawa K. (2005). Large-scale production of recombinant viruses by use of a large culture vessel with active gassing. *Human Gene Therapy* 16:1212-1218.

Ortiz GG, Pacheco-Moisés FP, Bitzer-Quintero OK, Ramírez-Anguiano AC, Flores-Alvarado LJ, Ramírez-Ramírez V, Macias-Islas MA, Torres-Sánchez ED. (2013). Immunology and Oxidative Stress in Multiple Sclerosis: Clinical and Basic Approach.

*Clin Dev Immunol* 2013:708659.

Pak BJ, Lee J, Thai BL, Fuchs SY, Shaked Y, Ronai Z, Kerbel RS, Ben-David Y. (2004). Radiation resistance of human melanoma analysed by retroviral insertional mutagenesis reveals a possible role for dopachrome tautomerase. *Oncogene* 23:30-38.

Panguluri SK, Yeakel C, Kakar SS. (2008). PTTG: an important target gene for ovarian cancer therapy. *J Ovarian Res* 1:6.

Pedraza L, Huang JK, Colman DR (2001). Organizing principles of the axoglial apparatus. *Neuron* 30:335-344.

Peles E, Salzer JL. (2000). Functional domains in myelinated axons. *Curr Opin Neurobiol* 10:558-565.

Pillai AM, Thaxton C, Pribisko AL, Cheng JG, Dupree JL, Bhat MA. (2009). Spatiotemporal ablation of myelinating glia-specific neurofascin (Nfasc NF155) in mice reveals gradual loss of paranodal axoglial junctions and concomitant disorganization of axonal domains. *J Neurosci Res* 87(8):1773-1793.

Preston GM, Carroll TP, Guggino WB, Agre P. (1992). Appearance of water channels

in *Xenopus* oocytes expressing red cell CHIP28 protein. *Science* 256:385-387.

Pringle NP, Mudhar HS, Collarini EJ, Richardson WD. (1992). PDGF receptors in the rat CNS: during late neurogenesis, PDGF alpha-receptor expression appears to be restricted to glial cells of the oligodendrocyte lineage. *Development* 115:535-551.

Rahn KA, Watkins CC, Alt J, Rais R, Stathis M, Grishkan I, Crainiceau CM, Pomper MG, Rojas C, Pletnikov MV, Calabresi PA, Brandt J, Barker PB, Slusher BS, Kaplin AI. (2012). Inhibition of glutamate carboxypeptidase II (GCPII) activity as a treatment for cognitive impairment in multiple sclerosis. *Proc Natl Acad Sci USA* 109:20101-20106.

Rasband, MN, Peles E, Trimmer JS, Levinson SR, Lux SE, Shrager P. (1999). Dependence of nodal sodium channel clustering on paranodal axoglial contact in the developing CNS. *J Neurosci* 19:7516-7528.

Renard M, Callewaert B, Malfait F, Campens L, Sharif S, del Campo M, Valenzuela I, McWilliam C, Coucke P, De Paepe A, De Backer J. (2013). Thoracic aortic-aneurysm and dissection in association with significant mitral valve disease caused by mutations in TGFB2. *Int J Cardiol* 165:584-587.

Rintoul GL, Bennett VJ, Papaconstantinou NA, Reynolds IJ. (2006). Nitric oxide inhibits mitochondrial movement in forebrain neurons associated with disruption of

mitochondrial membrane potential. *J Neurochem* 97:800-806.

Rios JC, Rubin M, St Martin M, Downey RT, Einheber S, Rosenbluth J, Levinson SR, Bhat M, and Salzer JL. (2003). Paranodal interactions regulate expression of sodium channel subtypes and provide a diffusion barrier for the node of Ranvier. *J Neurosci* 23:7001-7011.

Romero F, Multon MC, Ramos-Morales F, Dominguez A, Bernal JA, Pintor-Toro JA, Tortolero M. (2001). Human securin, hPTTG, is associated with Ku heterodimer, the regulatory subunit of the DNA-dependent protein kinase. *Nucleic Acids Res* 29:1300-1307.

Rosenbluth J, Mierzwa A, Shroff S. (2013). Molecular architecture of myelinated nerve fibers: leaky paranodal junctions and paranodal dysmyelination. *Neuroscientist* 19:629-641.

Roussos P, Katsel P, Davis KL, Bitsios P, Giakoumaki SG, Jogia J, Rozsnyai K, Collier D, Frangou S, Siever LJ, Haroutunian V. (2012). Molecular and genetic evidence for abnormalities in the nodes of Ranvier in schizophrenia. *Arch Gen Psychiatry* 69:7-15.

Stewart LR, Hall AL, Kang SH, Shaw CA, Beaudet AL. (2011). High frequency of known copy number abnormalities and maternal duplication 15q11-q13 in patients with

combined schizophrenia and epilepsy. *BMC Med Genet* 12:154.

Su KG, Banker G, Bourdette D, Forte M. (2009). Axonal degeneration in multiple sclerosis: the mitochondrial hypothesis. *Curr Neurol Neurosci Rep* 9:411-417.

Takahashi N, Sakurai T, Davis KL, Buxbaum JD. (2011). Linking oligodendrocyte and myelin dysfunction to neurocircuitry abnormalities in schizophrenia. *Prog Neurobiol* 93(1):13-24.

Takahara Y, Inatani M, Eto K, Inoue T, Kreymerman A, Miyake S, Ueno S, Nagaya M, Nakanishi A, Iwao K, Takamura Y, Sakamoto H, Satoh K, Kondo M, Sakamoto T, Goldberg JL, Nabekura J, Tanihara H. (2015). In vivo imaging of axonal transport of mitochondria in the diseased and aged mammalian CNS. *Proc Natl Acad Sci USA* 112:10515-10520.

Tanaka H, Ma J, Tanaka KF, Takao K, Komada M, Tanda K, Suzuki A, Ishibashi T, Baba H, Isa T, Shigemoto R, Ono K, Miyakawa T, Ikenaka K. (2009). Mice with altered myelin proteolipid protein gene expression display cognitive deficits accompanied by abnormal neuron-glia interactions and decreased conduction velocities. *J Neurosci* 29:8363-8371.

Tezel G. (2006). Oxidative stress in glaucomatous neurodegeneration: mechanisms and

consequences. *Prog Retin Eye Res* 25:490-513.

Trapp BD, Peterson J, Ransohoff RM, Rudick R, Mörk S, Bö L. (1998). Axonal transection in the lesions of multiple sclerosis. *N Engl J Med* 338:278-285.

Verkman AS, Hara-Chikuma M, Papadopoulos M. (2008). Aquaporins-new players in cancer biology. *J Mol Med* 86:523-529.

Volkmer H, Hassel B, Wolff JM, Frank R, Rathjen FG. (1992). Structure of the axonal surface recognition molecule neurofascin and its relationship to a neural subgroup of the immunoglobulin superfamily. *J Cell Biol* 118:149-161.

Wang Z, Moro E, Kovacs K, Yu R, Melmed S. (2003). Pituitary tumor transforming gene-null male mice exhibit impaired pancreatic beta cell proliferation and diabetes. *Proc Natl Acad Sci USA* 100:3428-3432.

Waxman SG, Bangalore L (2005). Myelin function and salutatory conduction. *In: Neuroglia*, Ed 2 (Kettenmann H, Ransom BR, eds), pp 273-284.

Yamamoto N, Yoneda K, Asai K, Sobue K, Tada T, Fujita Y, Katsuya H, Fujita M, Aihara N, Mase M, Yamada K, Miura Y, Kato T. (2001). Alterations in the expression of the AQP family in cultured rat astrocytes during hypoxia and reoxygenation. *Brain*

*Res Mol Brain Res* 90:26-38.

Yamazaki Y, Hozumi Y, Kaneko K, Fujii S, Goto K, Kato H. (2010).  
Oligodendrocytes: facilitating axonal conduction by more than myelination.  
*Neuroscientist* 16:11-18.

Zou H, McGarry TJ, Bernal T, Kirschner MW. (1999). Identification of a vertebrate  
sister-chromatid separation inhibitor involved in transformation and tumorigenesis.  
*Science* 285:418-422.

## Figure legends

### **Fig. 1. Efficiency of AAV-1, 5, 6, or DJ infection to oligodendrocytes in the corpus callosum.**

(A) Schematic drawing of AAV injection site. AAV-1, 5, 6, or DJ harboring the GFP gene were injected into a forebrain region in close proximity to the corpus callosum of 10-week-old C57BL/6 mice. (B) The representative coronal brain section showing AAV-mediated GFP expression (green) at 3 weeks after AAV injection. Scale bar; 200  $\mu$  m. (C) To check whether oligodendrocytes were infected with each AAV serotype, double staining with *in situ* hybridization for *PLP* mRNA (blue color) and immunostaining with anti-GFP antibody (brown color) was performed in the corpus callosum at 3 weeks after AAV injection. Arrowheads indicate double positive cells for *PLP* mRNA and GFP. The insets are magnified view of the cells indicated by arrows. Scale bar; 50  $\mu$  m. (D) The percentage of *PLP* mRNA<sup>+</sup> GFP<sup>+</sup> double-positive cells / total GFP<sup>+</sup> cells in the corpus callosum for each respective serotype (n = 2-3 each).

### **Fig. 2. Measurement of latency in response to electric stimulation of the motor cortex.**

(A, B) Schematic drawing and time course of the experiment. To examine whether site-directed loss of paranodal junction causes a delay in the forelimb muscle response against stimulus of the motor cortex, an electrode was inserted into the motor cortex of 7-week-old *NF155<sup>Flox/Flox</sup>* mouse, and then AAV5-EGFP-2A-Cre was injected into the internal capsule of the mice one week after the electrode insertion. Recording electrode was placed in triceps of forelimb. EMG was measured in response to electric stimulation of the motor cortex every week until 20-weeks of age. (C) Representative data of EMG in response to electric stimulation of the motor cortex. The onset latency was defined as the time between the stimulus (arrow) and the initiation of the first wave (arrowhead).

**Fig. 3. AAV-Cre-induced loss of paranodal junctions in the internal capsule.**

(A) Schematic drawing of AAV5-EGFP-2A-Cre injection site (green). (B) To check whether oligodendrocytes in the internal capsule were infected with AAV, double staining with *in situ* hybridization for *PLP* mRNA (blue color) and immunostaining with anti-GFP antibody (brown color) was performed in the internal capsule 12 weeks after AAV injection. Arrowheads indicate double positive cells for *PLP* mRNA and GFP. The inset is a magnified view of the cell indicated by an arrow. Scale bar; 50  $\mu$  m. (C) Immunofluorescence staining with anti-Na<sup>+</sup> channel (red) and anti-Caspr (green)

antibodies of the sections containing internal capsule region of the control (left panel) or *NF155<sup>Flox/Flox</sup>* (right panel) mice at 12 weeks after the injection of AAV5-EGFP-2A-Cre. Scale bar; 20  $\mu$  m. (D) Quantification of the length of Caspr-positive paranodes in the control (left panel) and *NF155<sup>Flox/Flox</sup>* (right panel) mice injected with AAV-Cre (n = 3 each). Significant levels; \*p<0.01 vs. control mice (Student's t-test, p = 0.0060, t = 5.319, df = 4).

**Fig. 4. Electrophysiological analyses of EMG in *NF155<sup>Flox/Flox</sup>* mice injected with AAV5-EGFP-2A-Cre.**

Latency was measured in response to electric stimulation of the motor cortex every week until 20-weeks of age. Significant levels; \*p<0.05 vs. control mice (Tukey's test, 17w: p = 0.0253, 18w: p = 0.0235).

**Fig. 5. Paranodal junctions were disrupted in the optic nerves of *Plp-NF155<sup>Flox/Flox</sup>* mice.**

(A) Optic nerve sections prepared from *Plp-NF155<sup>+ /FloX</sup>* and *Plp-NF155<sup>Flox/Flox</sup>* mice 60 days after tamoxifen administration were immunostained with anti-NF155 (upper panel) and anti-Caspr (lower panel) antibodies. The inset is a magnified view of the

immunolabeling indicated by arrows. Scale bar; 20  $\mu$  m. (B, C) Quantification of the number and length of paranodes immunolabeled by anti-NF155 (B) or anti-Caspr (C) antibodies in *Plp-NF155<sup>+ /Flo x</sup>* and *Plp-NF155<sup>Flo x /Flo x</sup>* mice (n = 3 each). Significant levels; \*p<0.05, \*\*p<0.01, \*\*\*p<0.001 vs. *Plp-NF155<sup>+ /Flo x</sup>* mice (Student's t-test, number of NF155: p = 0.0006, t = 10.00, df = 4; length of NF155: p = 0.0437, t = 2.682, df = 5; number of Caspr: p = 0.0070, t = 5.091, df = 4; length of Caspr: p = 0.0026, t = 6.719, df = 4).

**Fig. 6. Microarray analysis with total RNA prepared from the retina of *Plp-NF155<sup>+ /Flo x</sup>* or the *Plp-NF155<sup>Flo x /Flo x</sup>* mice.**

To investigate neuronal gene expression responding to paranodal opening, total RNA was isolated from the retina of *Plp-NF155<sup>+ /Flo x</sup>* and *Plp-NF155<sup>Flo x /Flo x</sup>* mice (n = 2 per group) 60 days after tamoxifen administration and proceeded to microarray analysis. (A) A scatter plot of gene expression levels in response to the ablation of *NF155*. The normalized intensity values were represented by  $\log_2$ . The identified genes focused in this study were indicated by red (up-regulation) and blue (down-regulation) dots. The green line represents a 2-fold change. (B, C) The identified gene expression levels in the *Plp-NF155<sup>+ /Flo x</sup>* and *Plp-NF155<sup>Flo x /Flo x</sup>* mice 60 days after tamoxifen administration were confirmed by qRT-PCR (n = 4-5 each). Significant levels; \*p<0.05, \*\*p<0.01 vs. *Plp-NF155<sup>+ /Flo x</sup>* mice (Student's t-test, *Dcn*: p = 0.0270, t = 2.702, df = 8; *Myh11*: p =

0.0277,  $t = 2.769$ ,  $df = 7$ ; *Pttg1*:  $p = 0.0063$ ,  $t = 3.670$ ,  $df = 8$ ; *Dcn*:  $p = 0.0137$ ,  $t = 3.145$ ,  $df = 8$ ; *Tti2*:  $p = 0.0276$ ,  $t = 2.772$ ,  $df = 7$ ; *Aqp3*:  $p = 0.0127$ ,  $t = 3.324$ ,  $df = 7$ ).

**Fig. 7. qRT-PCR analysis of the selected gene expression in the retina of *Plp-NF155<sup>Flox/Flox</sup>* and *CST-KO* mice.**

The expression level of selected genes in the retina of 4- or 6-week-old *CST-KO* mice ( $n = 4-5$  each) or *Plp-NF155<sup>Flox/Flox</sup>* mice ( $n = 4-5$  each) 40 or 60 days after tamoxifen administration was compared to that of the *Plp-NF155<sup>+Flox</sup>*. (A, C, E, G) The expression levels of *Dcn* (A), *Myh11* (C), *Pttg1* (E), and *Aqp3* (G) in *Plp-NF155<sup>Flox/Flox</sup>* mice were determined by qRT-PCR. Significant levels; \* $p < 0.05$ , \*\* $p < 0.01$  vs. *Plp-NF155<sup>+Flox</sup>* mice [Student's t-test, *Dcn* (6w):  $p = 0.0270$ ,  $t = 2.702$ ,  $df = 8$ ; *Myh11* (6w):  $p = 0.0277$ ,  $t = 2.769$ ,  $df = 7$ ; *Pttg1* (6w):  $p = 0.0063$ ,  $t = 3.670$ ,  $df = 8$ ; *Aqp3* (6w):  $p = 0.0127$ ,  $t = 3.324$ ,  $df = 7$ ]. (B, D, F, H) The expression level of *Dcn* (B), *Myh11* (D), *Pttg1* (F), and *Aqp3* (H) in *CST-KO* mice was also examined by qRT-PCR. Significant levels; \* $p < 0.05$ , \*\* $p < 0.01$  vs. wild-type mice [Student's t-test, *Dcn* (4w):  $p = 0.0003$ ,  $t = 6.123$ ,  $df = 8$ ; *Dcn* (6w):  $p = 0.0314$ ,  $t = 2.605$ ,  $df = 8$ ; *Myh11* (6w):  $p = 0.0454$ ,  $t = 2.368$ ,  $df = 8$ ].

**Fig. 8. *Pttg1* was also up-regulated in the cerebral cortex by the collapse of**

**paranodal junctions.**

(A, B) To examine whether the *Pttg1* expression was changed in the cerebral cortex as well, qRT-PCR was performed in the *Plp-NF155<sup>Flox/Flox</sup>* (A, n = 4-5 each) and *CST-KO* mice (B, n = 4-5 each). Significant levels; \*p<0.05 vs. *Plp-NF155<sup>+/Flox</sup>* mice [Student's t-test, *Plp-NF155<sup>Flox/Flox</sup>* (60 days after tamoxifen treatment): p = 0.0183, t = 2.954, df = 8]. ns; Not significant. (C) Double labeling with *in situ* hybridization for *Pttg1* mRNA (blue color) and immunostaining with anti-NeuN antibody (brown color) was performed in the cerebral cortex of 10-week-old C57BL/6 mice. Higher magnification view of the boxed area in the upper panel is shown in the under panel. Scale bar; 100  $\mu$  m. (D) The percentage of *Pttg1* mRNA<sup>+</sup> or <sup>-</sup> cells/ NeuN<sup>+</sup> cells were quantified in the cerebral cortex (n = 3).

**Fig. 9. CNV of the *Aqp3* gene was found in the schizophrenic patients, whose expression was altered in the *Plp-NF155<sup>Flox/Flox</sup>* mice.**

(A) Schematic drawing of the CNV positions in the *Aqp3* locus. Duplications were shown as blue bars (n = 1699). (B) To examine whether the *Aqp3* expression was changed in the cerebral cortex of *Plp-NF155<sup>Flox/Flox</sup>* mice (n = 4-5 each), qRT-PCR was performed in the mice 40 or 60 days after tamoxifen administration. Significant levels; \*p<0.05 vs. *Plp-NF155<sup>+/Flox</sup>* mice (Student's t-test, p = 0.0133, t = 3.288, df = 7). (C)

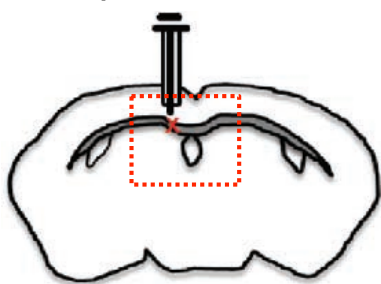
Double labeling with *in situ* hybridization for *Aqp3* mRNA (blue color) and immunostaining with anti-NeuN antibody (brown color) was performed in the cerebral cortex of 10-week-old C57BL/6 mice. The inset shows magnified view of the cell indicated by an arrow. Scale bar; 50  $\mu$  m. (D) The percentage of *Aqp3* mRNA<sup>+</sup> or <sup>-</sup> cells/ NeuN<sup>+</sup> cells were quantified in the cerebral cortex (n = 3).

**Table 1.** Primer sequences used for RT-PCR and qRT-PCR.

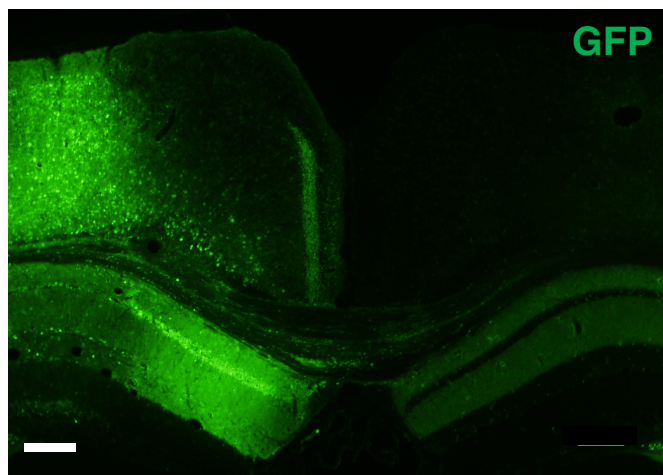
Gene symbol	Accession No.	primer	sequences (5' to 3')
<i>Dcn</i>	NM_001190451.2	Forward	GATTTTCCACCCGACACAAC
		Reverse	ATGAGGAACATTGGCCAGAC
<i>Myh11</i>	NM_001161775	Forward	GTGACCTGCTTTTGGAGAGC
		Reverse	GCCTGTTCTTTGGTCTGAGC
<i>Pttg1</i>	NM_013917.2	Forward	TGGCTTCTAAGGATGGGTTG
		Reverse	GTGGCAATTCAACATCCAGA
<i>Dct</i>	NM_010024	Forward	TGTGCAAGATTGCCTGTCTC
		Reverse	GTTGCTCTGCGGTTAGGAAG
<i>Tti2</i>	NM_001199988.1	Forward	TCACCTGTACATGCCTGAGC
		Reverse	CAGGGTTTCCAGGATCTTCA
<i>Aqp3</i>	NM_016689	Forward	ATTCTGGCTATGCCGTCAAC
		Reverse	AAACTTGGTCCCTTGCCTTT
<i>β-actin</i>	NM_007393	Forward	TGACAGGATGCAGAAGGAGA
		Reverse	GCTGGAAGGTGGACAGTGAG

A

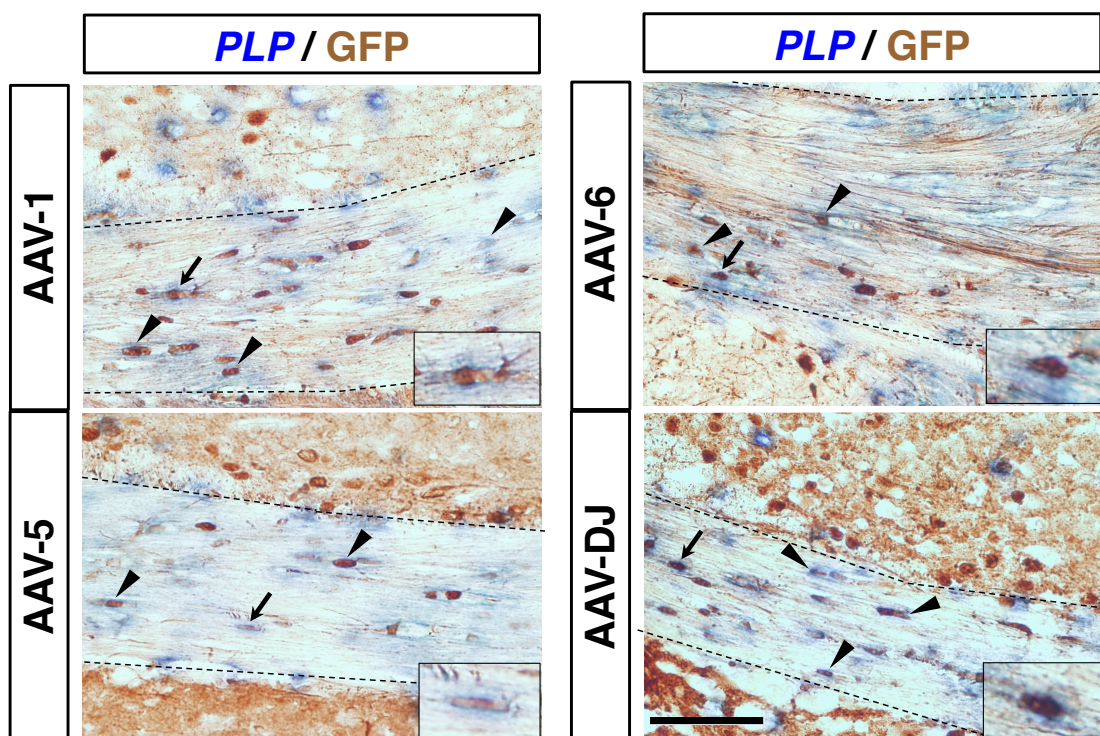
Corpus callosum



B



C



D

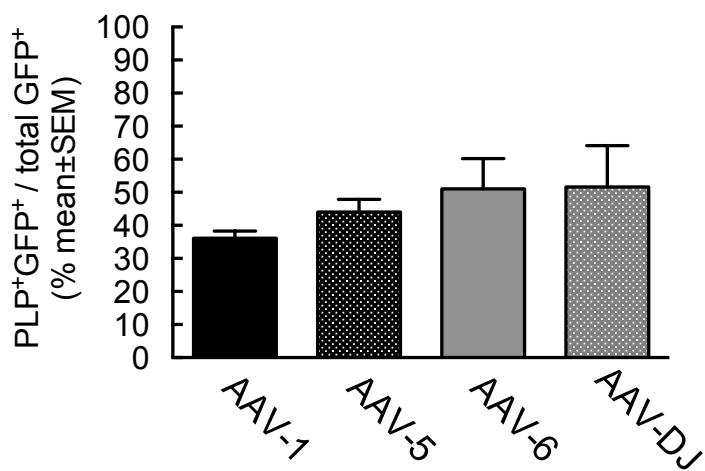
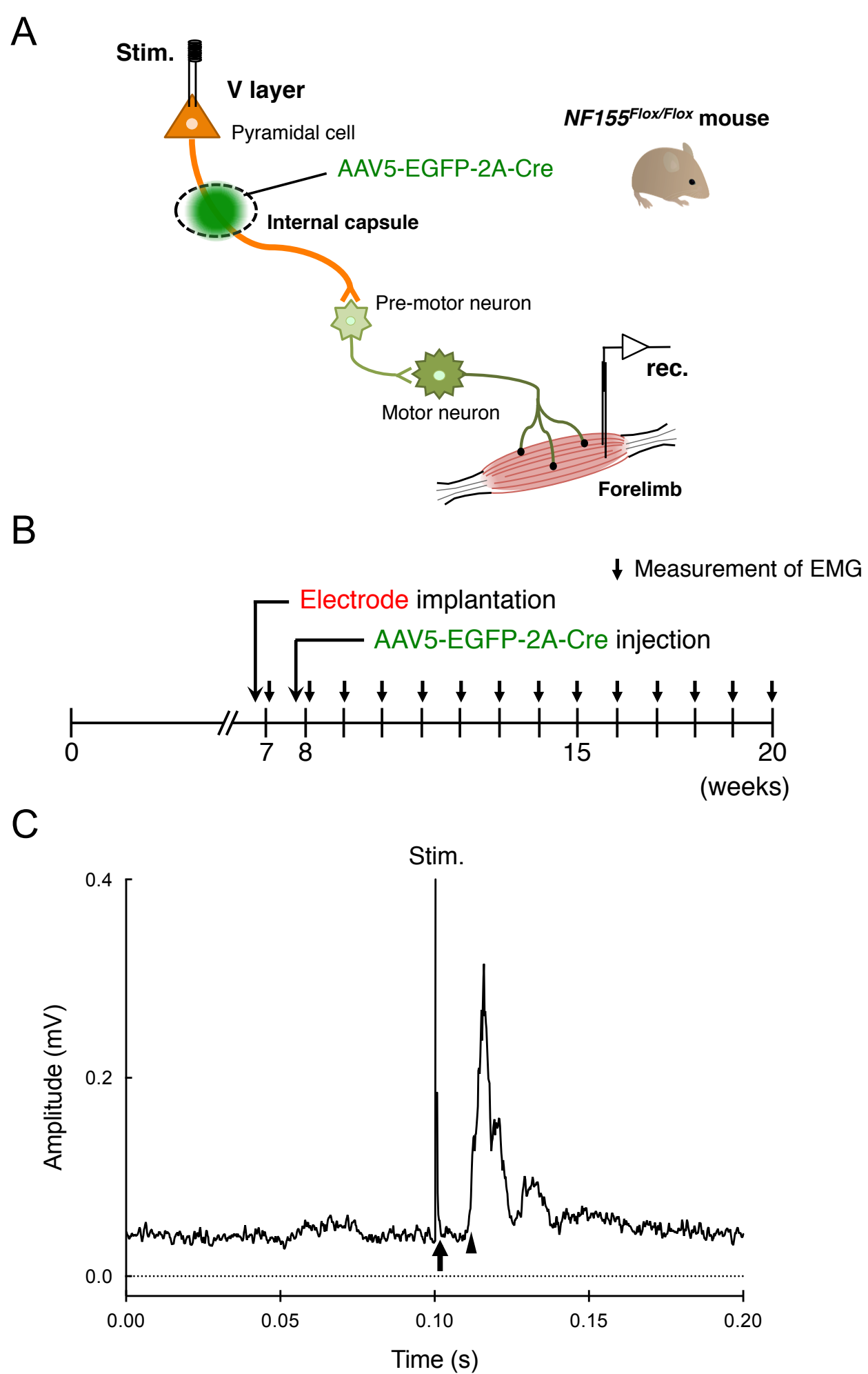
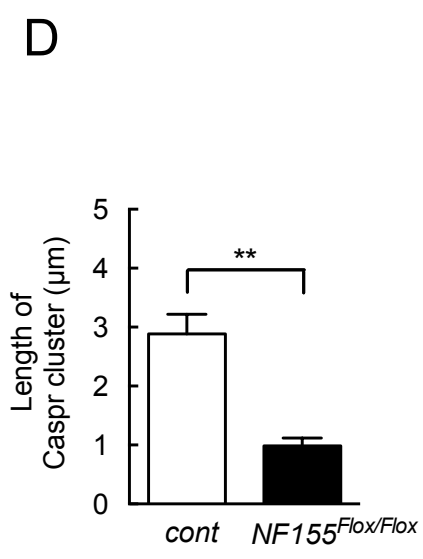
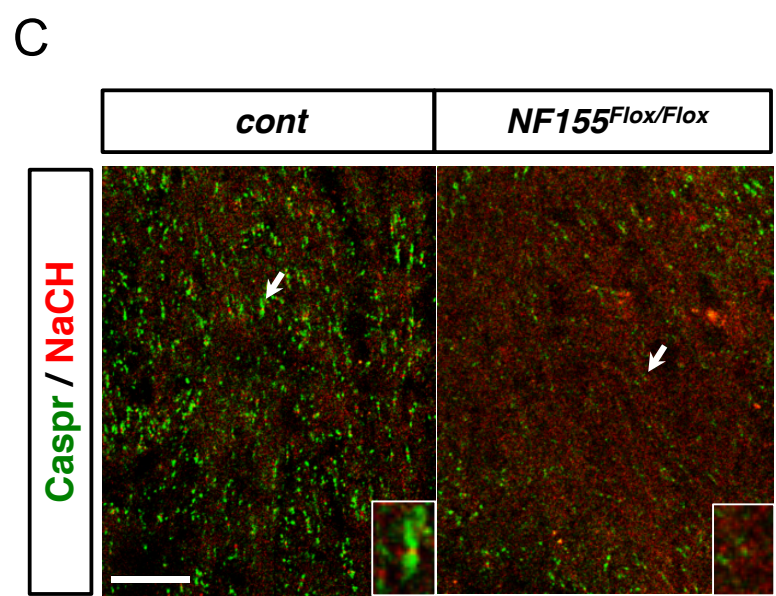
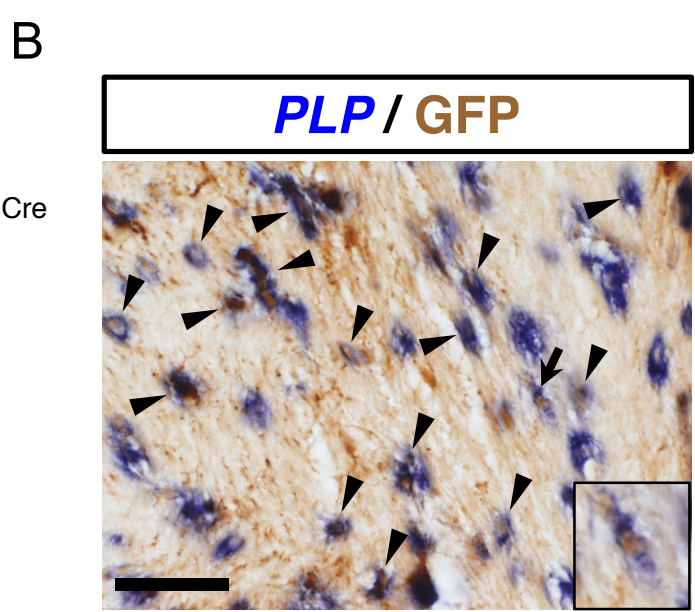
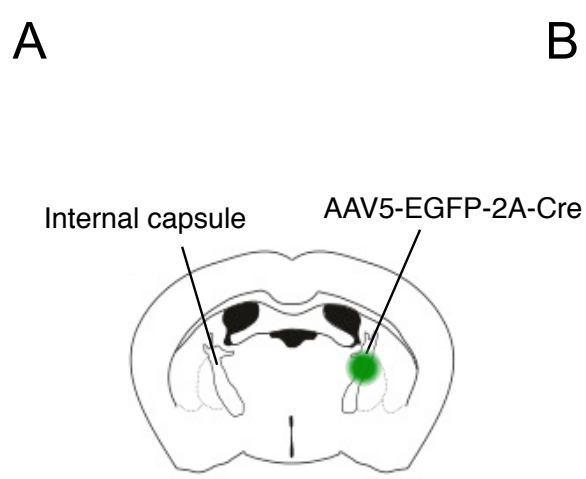


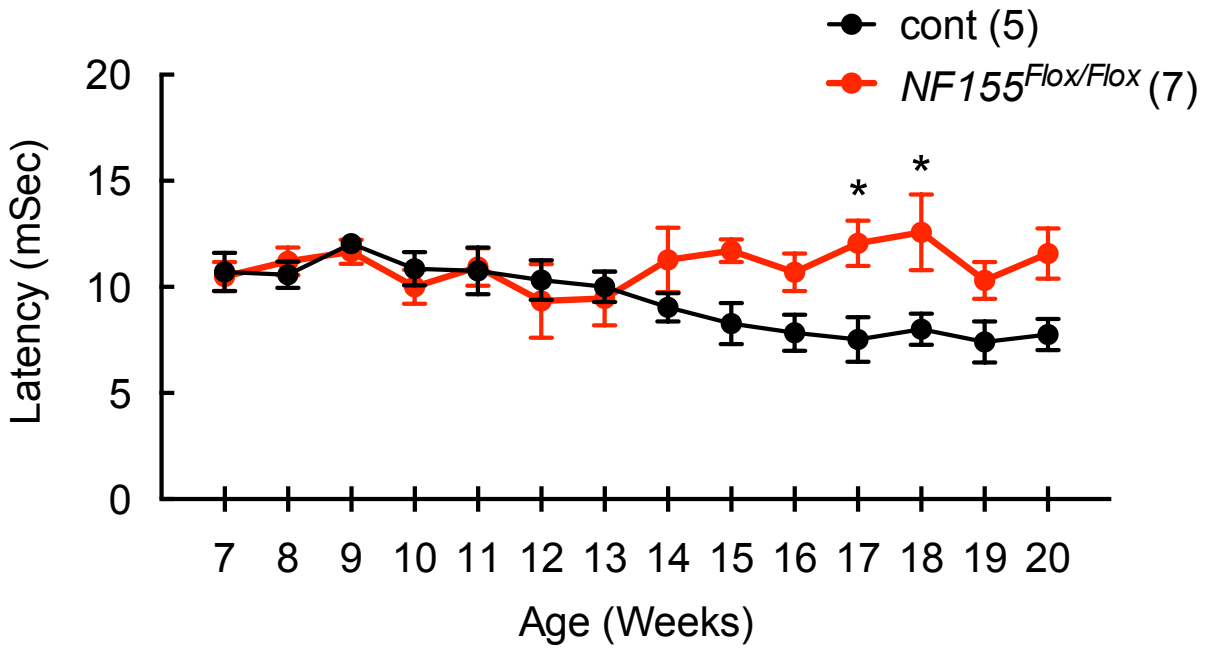
Fig. 1



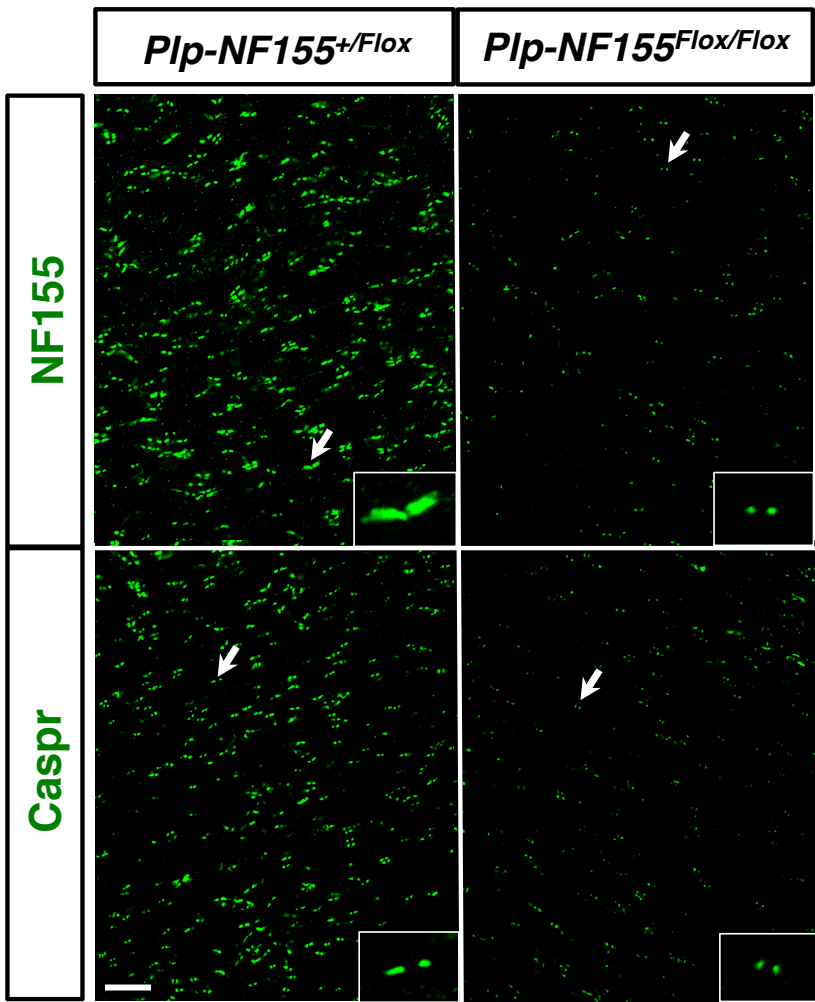
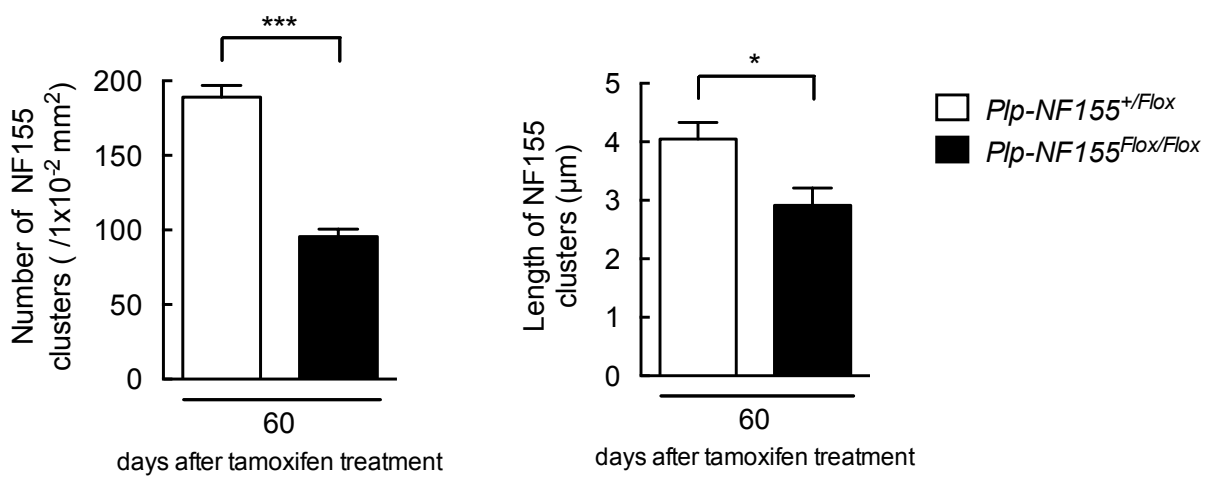
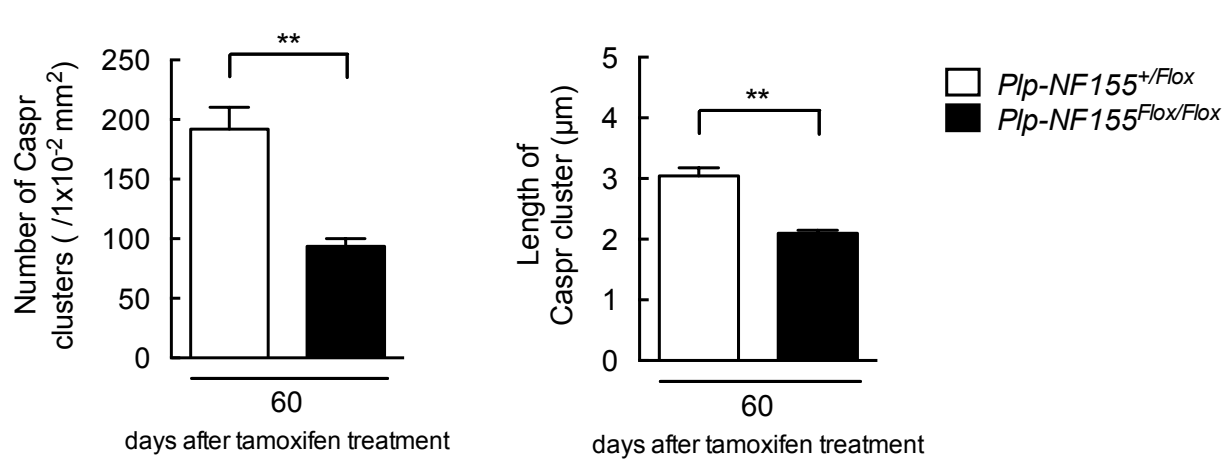
**Fig. 2**



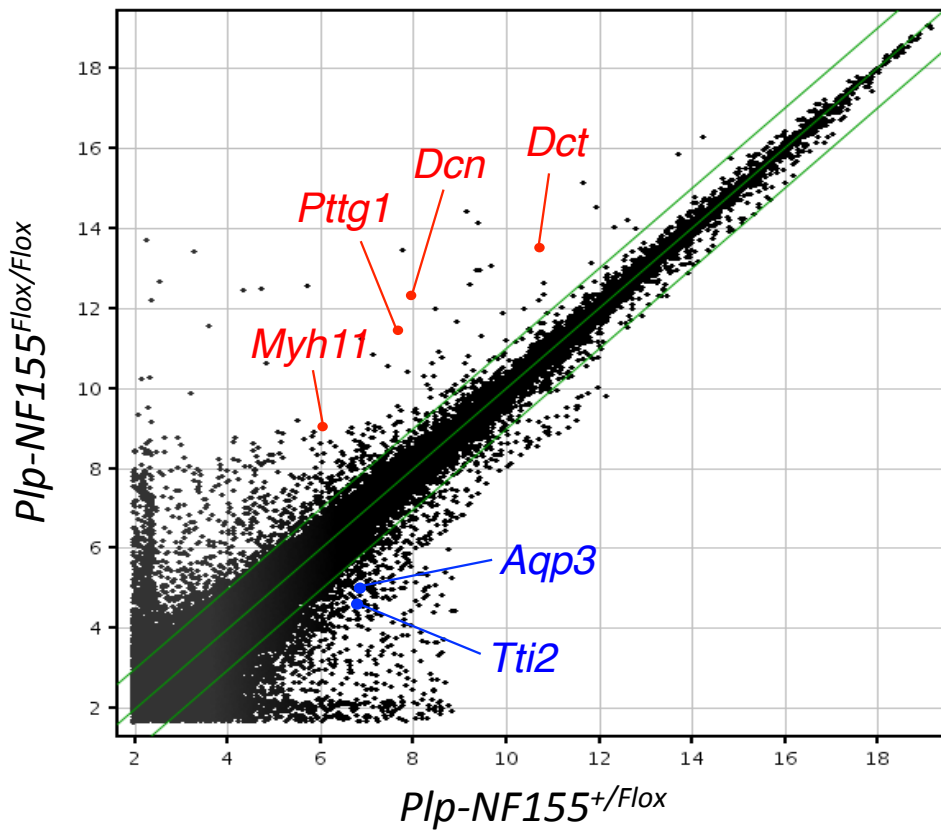
**Fig. 3**



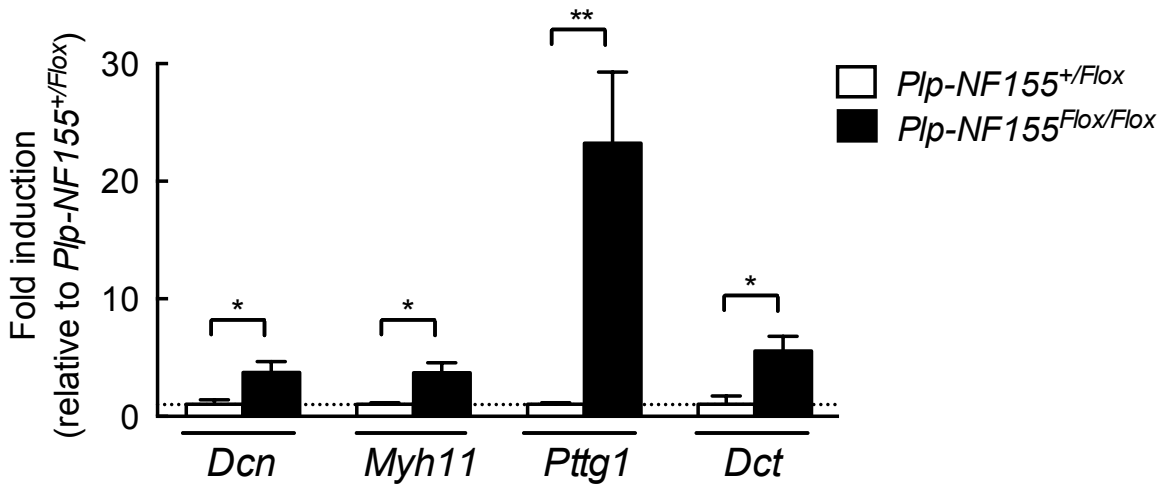
**Fig. 4**

**A****B****C****Fig. 5**

A



B



C

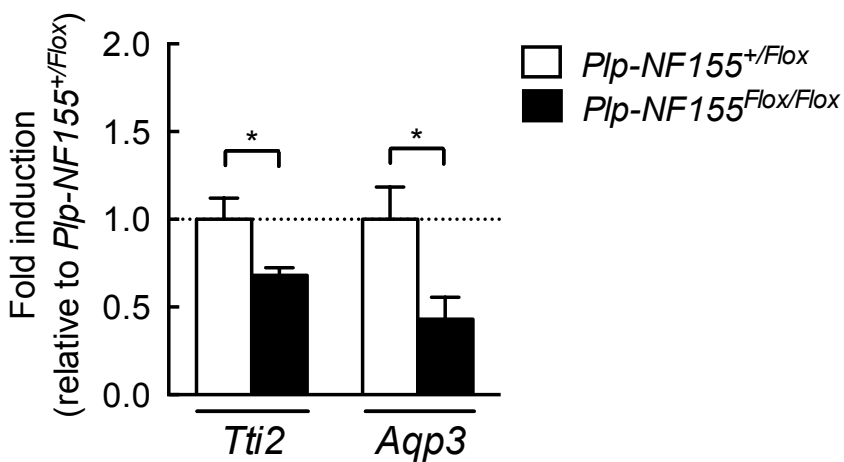
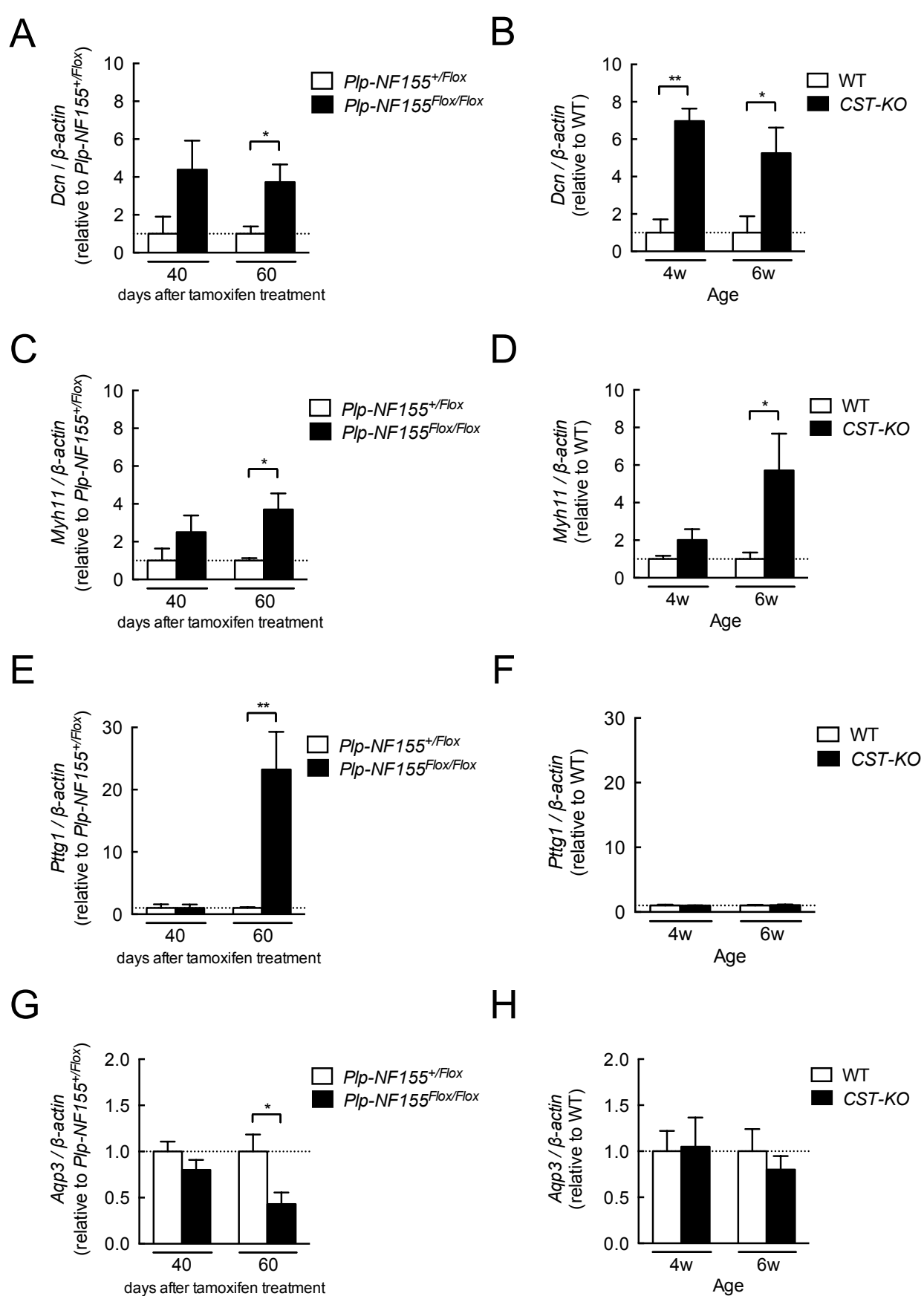
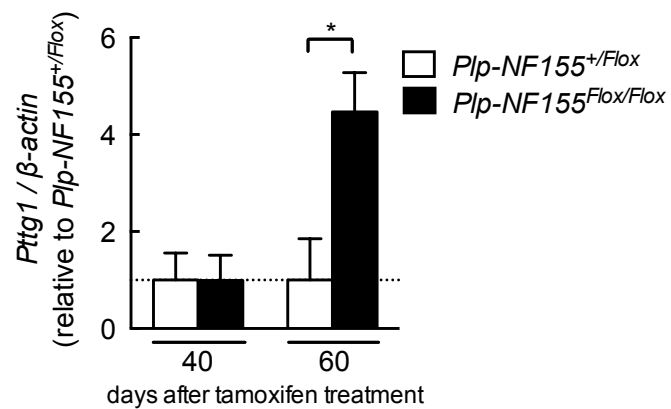
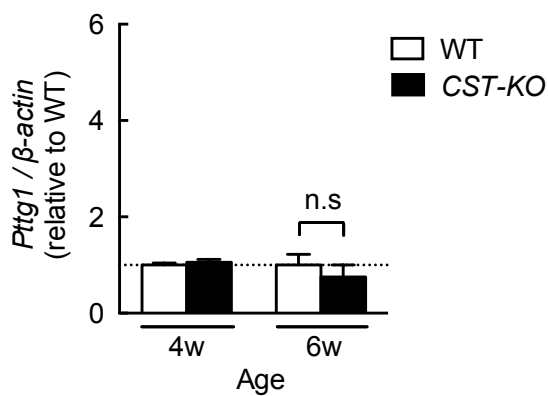
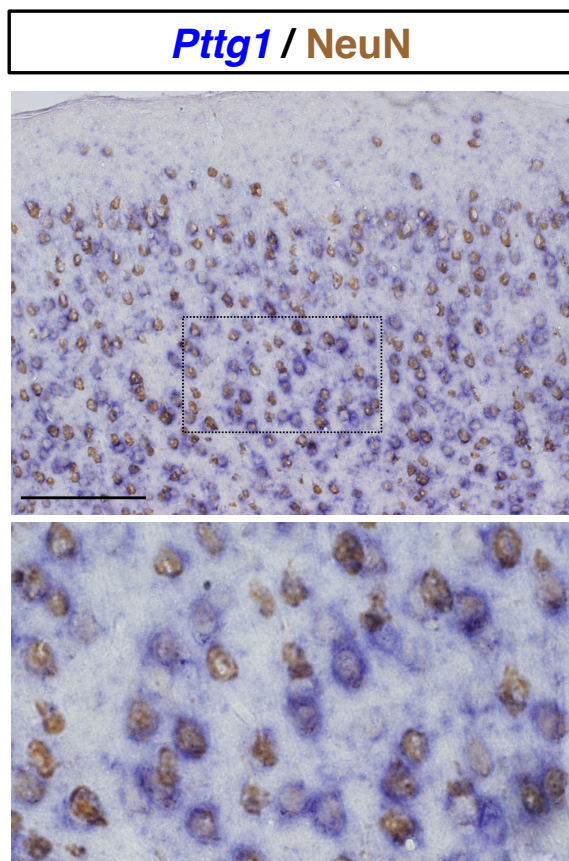
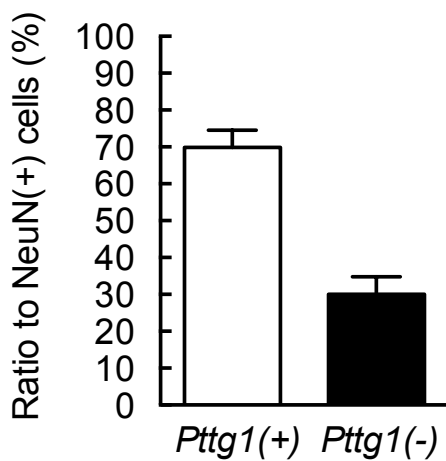


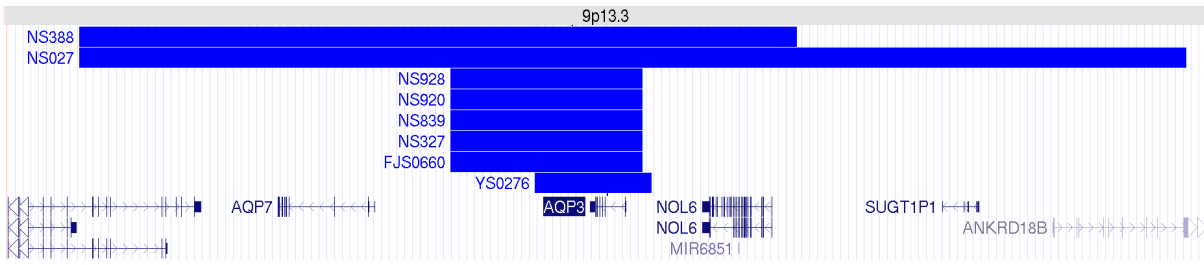
Fig. 6



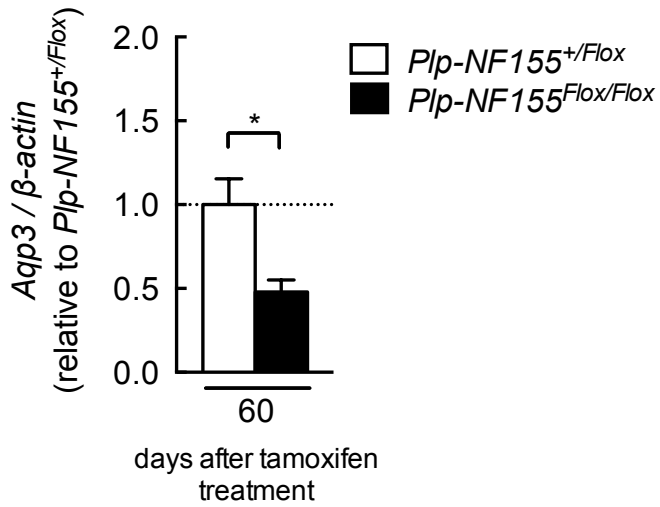
**Fig. 7**

**A****B****C****D****Fig. 8**

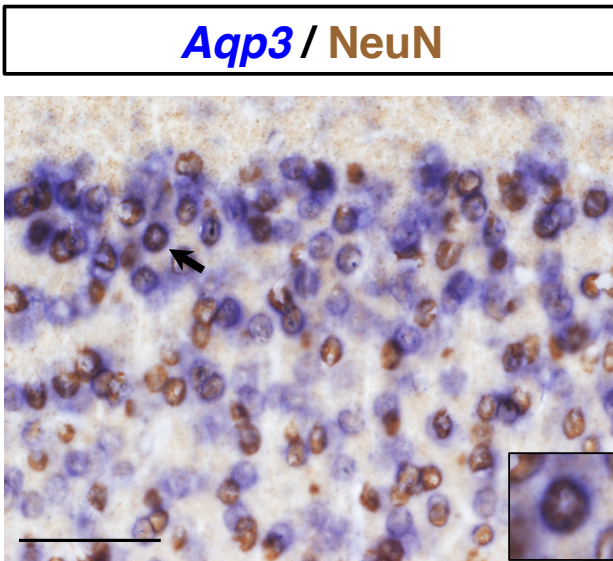
A



B



C



D

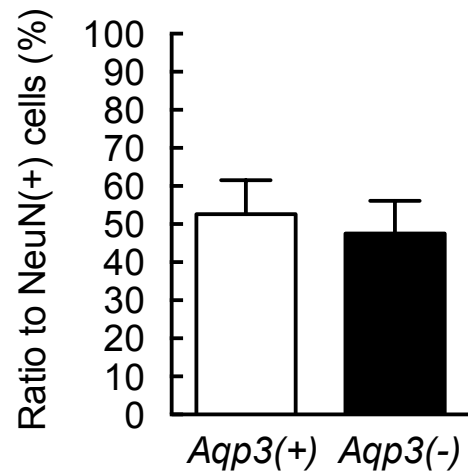


Fig. 9